Process-based Modelling of Late Quaternary Morphology and Stratigraphy of the Northern Adriatic Basin

Master's Thesis:
MSc track Petroleum Engineering and Geosciences
Delft University of Technology
The Netherlands

August 13, 2009

Meron Okbay Teklesenbet
Student number: 1379445

Abstract

The thesis is devoted to calibration of a process-based numerical model and its application to simulation of the Late Quaternary history and stratigraphy of the Northern Adriatic Sea. Tests aimed at assessing the sensitivity of the model to initial and boundary conditions were conducted, based on geomorphologic and stratigraphic data culled from literature. Based on these tests, wave-generated erosion and diffusion coupled with current-induced removal and transportation algorithms were adopted to simulate intensification of the Western Adriatic Coastal Current (WACC) by the Bora Wind during the Late Holocene. Different scenarios have been assessed to examine the model's ability to reproduce the stratigraphic architecture of the Adriatic Basin. Model results for the prodelta of the Po River at the north-western low-gradient shelf are represented by a continuous subaqueous delta, which forms an elongated coast-hugging deposit. The central Apennine part of the western shelf, which has a comparatively steep gradient, is characterized by the presence of fluvio-deltaic lobes deposited by the Apennine Rivers. The sediment budget has been calculated based on the isopach maps of modelled stratigraphy. A total sediment mass of abut 800 Gt was supplied to the basin over the time span corresponding to TST and HST (~19 kyr). Volumetric estimates indicate that roughly 87% of the supplied sediments have been preserved on the shelf. This suggests an export of ~13% to the MAD and to the southern part of the basin. The result is compatible with literature, where 10% of the sediment has been reported to move south of the Gargano promontory. Over the past 5.5 kyr, 256 Gt of sediment has been preserved on the shelf and is stored in the HST, corresponding to an average rate of deposition about 46 Mt yr^{-1}, which is ~4 Mt yr^{-1} more than study reports. The rate of fluvial sediment supply (52 Mt yr^{-1}) during formation of the HST suggests an export of ~6 Mt yr^{-1} to deeper parts of the basin below the effective hydrodynamic base.

Table of Content

List of Figures

List of Tables

List of abbreviations and symbols

Symbol	Definition
BP	Before Present
C	Cohesive (clay) fractions
ca.	Estimated year
GSDs	Grain size distributions
Gt	Giga (10^9) ton
HST	Highstand Systems Tracts
kyr	Thousands of years
LGM	Last Glacial Maximum
Mt	Mega (10^6) ton
MAD	Middle Adriatic Deep
S	Sortable silt fractions
SPM	suspended particulate matter
TST	Transgressive Systems Tracts
WACC	West Adriatic Coastal Current
µm	micro-meter (10^{-6})

Chapter 1: Introduction

The research project is a partial fulfilment for the master program of Applied Earth Sciences at the Delft University of Technology. The project is devoted to calibration and application of a "process-based numerical model" to simulate the Late Quaternary history and stratigraphy of the Northern Adriatic Sea. The model is designed to simulate sediment distribution and stratigraphic response of a continental shelf in a high energetic hydrodynamic activity, subjected to waves and currents. The Adriatic is an ideal basin for the application of the model, and it is the focus of the project to simulate and assess the morphological and stratigraphical developments of the north-western Adriatic shelf deposits. The result of the model has basically captured the essence of sediment transport processes and stratigraphic architecture of the Adriatic basin; and the model parameters can be alternatively turned on/off to perceive each factor's influence on the stratigraphy of the basin. Further the model can be used in predicting and monitoring a coastal zone of a sedimentary basin subjected to storm events.

The Adriatic basin is located east of Italy between 120 to 190 of longitude, and 400 to 460 of latitude. It is an epicontinental basin, about 800km long and 200km wide, Pliocene to Quaternary in age. Material exchange with the Mediterranean Sea takes place on its southern mouth through the Strait of Otranto, Figure 2-1. The Northern Adriatic is a shallow basin with a water depth below 100m, and has a very gentle slope of about 0.020. Depressions that are about 250m and 1200m deep, respectively, occupy the middle and the southern regions of the Adriatic basin. Rivers discharging to the Adriatic basin drain three types of terrain. The eastern drainage area, the "Croatian Coast" contributes fairly large amount of freshwater and negligible sediment input due to the large amounts of karstified carbonates. Rivers that drain the Alpine watersheds have a seasonally altering low sediment yield. Rivers on the east coast of Italy drain the more easily erodible Apennine Mountains which are the main supply of sediments to the Adriatic basin (Cattaneo et al. 2003 and Brommer 2009). The Po River tributaries drain both Alpine and Apennine mountains, and it is the largest sediment supplier to the Adriatic (~15 to 19 Mt yr^{-1}). The remaining Apennine Rivers are relatively short, steep and classified as small mountain rivers. As a group, they account for a sediment supply of about 32 Mt yr^{-1}, which is ~60% of Adriatic supply. Wind intensified western-coast current, the Western Adriatic Coastal Current (WACC) flows southward with a long-term average maximum speed of 0.2 ms^{-1}. The WACC is the main sediment transport mechanism along the western shelf, which carries the sediments southward where it eventually accumulates as far south as the Gargano Promontory, (Cattaneo et al. 2003, Frignani et al. 2005, and Harris et al. 2008).

During the simulation of the Adriatic sedimentary architecture, the project has covered many topics starting from the constrained Adriatic system description and continental-marine boundary conditions going through the application and interpretation of the different scenarios of the model. The report is presented mainly into two parts, where

the first part covers the literature review of the Adriatic basin and sensitivity tests of the numerical model in a synthetic basin; to comprehend the effects of the model's factors on transportation and sedimentation processes. The second part deals with the calibration and application of the model to simulate and address the detailed depositional process of the Western Adriatic mud deposits along the Apennine margin. Geomorphologic and stratigraphic developments, depositional cross-sections and spatial grain-size dispersion analysis, sedimentation rate estimation and discussion of the results are the core of the project. In each part, the uncertainty is analyzed and addressed to the constraint parameters that could be the possible sources. Finally yet importantly, the report includes recommendations for a further development of the numerical model on the influential factors that could alter the entire model of hydrodynamic and stratigraphic development of the Adriatic deposits.

The model has basically revealed an intuitive understanding on the transportation and depositional processes of the Adriatic basin that can be traced and analyzed at various spatial and temporal scales. The results are reasonable and suggest that it is possible to simulate the Late Quaternary stratigraphic history and the sediment flux record of the Adriatic basin; which are also comparable with literature reports. The thesis is presented in a sequential order as it was performed during the research.

Chapter 2: Literature Review

This chapter comprises a summary of the literature on the Adriatic basin. The main focus lies on reports that can be used as an input data for the process based numerical model. The subjects of: Regional geology of the Alpine and Apennine domains and the stratigraphy of the Adriatic basin; sediment source and characteristics; hydrodynamics and sediment transportation pattern; sedimentation and preservation potential of the deposits on the Western Adriatic shelf are summarized.

2.1 Regional Geology

The Adriatic Sea occupies the foreland of the Apennine and Dinaric thrust belts, formed by the collision of African and European plates during the Miocene to early Pleistocene. The Western side of the northern and central Adriatic is a foredeep basin, Pliocene-Quaternary in age that represents the most recent series of foredeep basins formed during the Apennine orogenesis and migrated eastwards, Figure 2-2. The eastern margin of the Apennine chain resulted in the development of a complex foreland basin system since the early Miocene, (Cattaneo et al. 2003 and Royden et al. 1987).

The general structural setting of the hinterland of Italy can be divided into four stratigraphic zones; which extend from west to east in the Apennine system and from north to south in the Maghrebian system. These consist of internal zone of the Apennine thrust system; external zone of the Apennine and Maghrebian thrust systems; Pliocene-Pleistocene foredeep and Mesozoic carbonate foreland, (Holton, 1999). The stratigraphic zones are composed of:

- The internal (western) portion of the Apennine system is made up of stacked, imbricate thrust sheets ranging in age from Late Triassic to Upper Miocene, dominantly containing Mesozoic carbonates and Miocene sandstone.
- The Apennine - Maghrebian thrust system is composed of Miocene and Lower-Middle Pliocene foredeep turbidite sandstones. It also consists of a thin section of Messinian evaporites and Lower Pliocene shale.
- The Pliocene-Pleistocene foredeep contains sandstones that cover the northern-central Adriatic and the Po basin of the northern Italy.
- The Mesozoic foreland is a relatively undisturbed carbonate platform. On the shore, various thicknesses of Miocene and in some cases a thin section of Pliocene-Pleistocene sediments overlie the formations. Offshore, the Miocene section is absent and the Mesozoic foreland sequence is overlain by sediments of the Pliocene-Pleistocene foredeep, (Holton, 1999).

2.2 Morphology of the Adriatic basin

The modern Adriatic basin (Pliocene-Quaternary foredeep basin) has an arcuate shape with two distinct depocenter separated by a structural high in the area of Ancona, Figure 2-1. It is a narrow epicontinental basin (ca. 200x800 km). The northern Adriatic

has a low longitudinal topographic gradient (ca 0.02^0), whereas the maximum shelf gradient along the central Adriatic is in the order of 0.5^0 (Cattaneo et al. 2003). The central Adriatic reaches a maximum depth of 260m, and is characterized by a narrower shelf with a localized bathymetric irregularities that are expressions of structural highs offshore the Punta Penna, the Tremiti Islands and the Gargano promontory. The southern Adriatic, beyond the Pelagosa sill, reaches a depth of about 1200m and is flanked by a steep slope and narrow shelf. Exceptionally the area just south of the Gargano promontory, the shelf broadens to about 70 to 80 km, (Cattaneo et al. 2003).

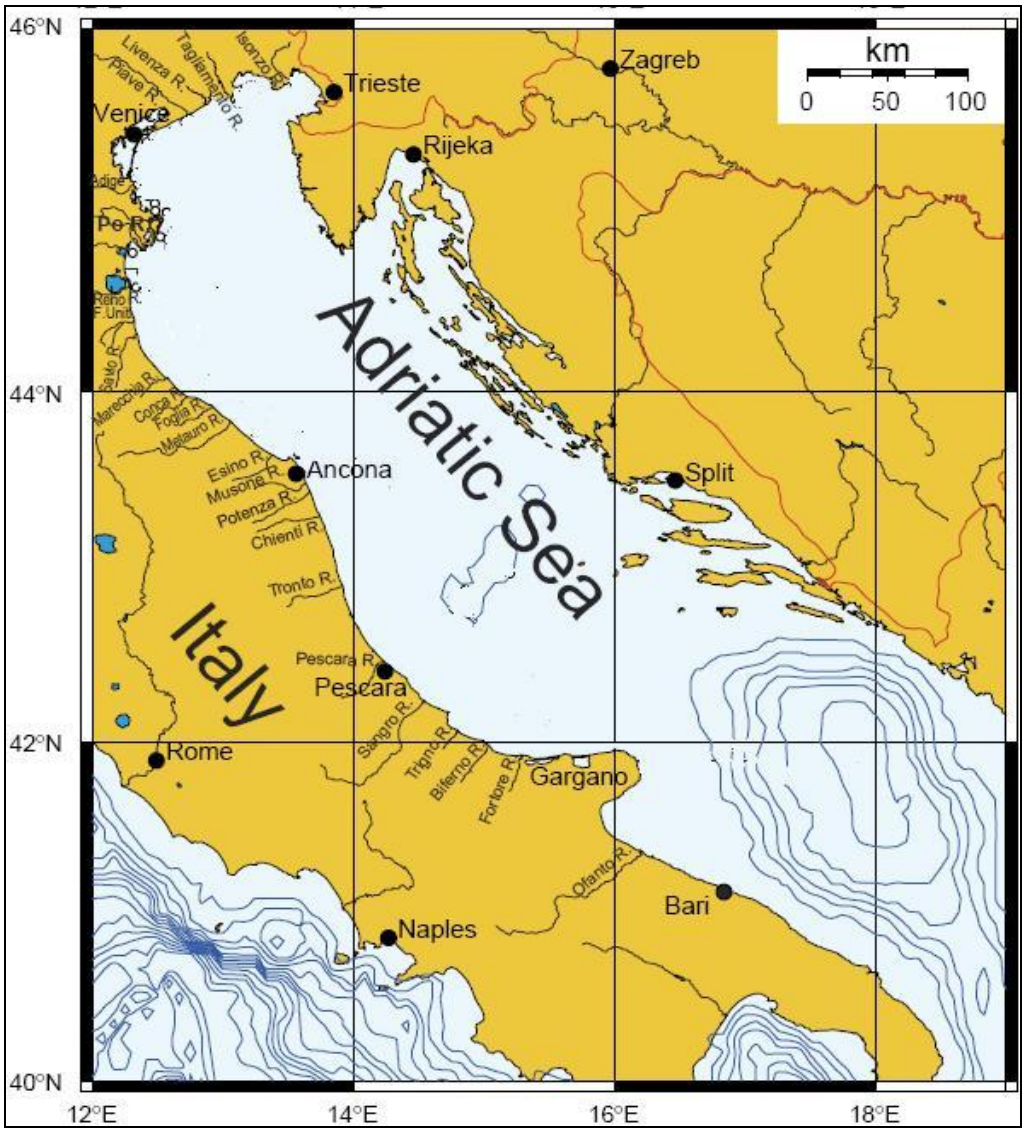

Figure 2-1: Geographic and drainage map of the Adriatic Sea, (Frignani et al. 2005).

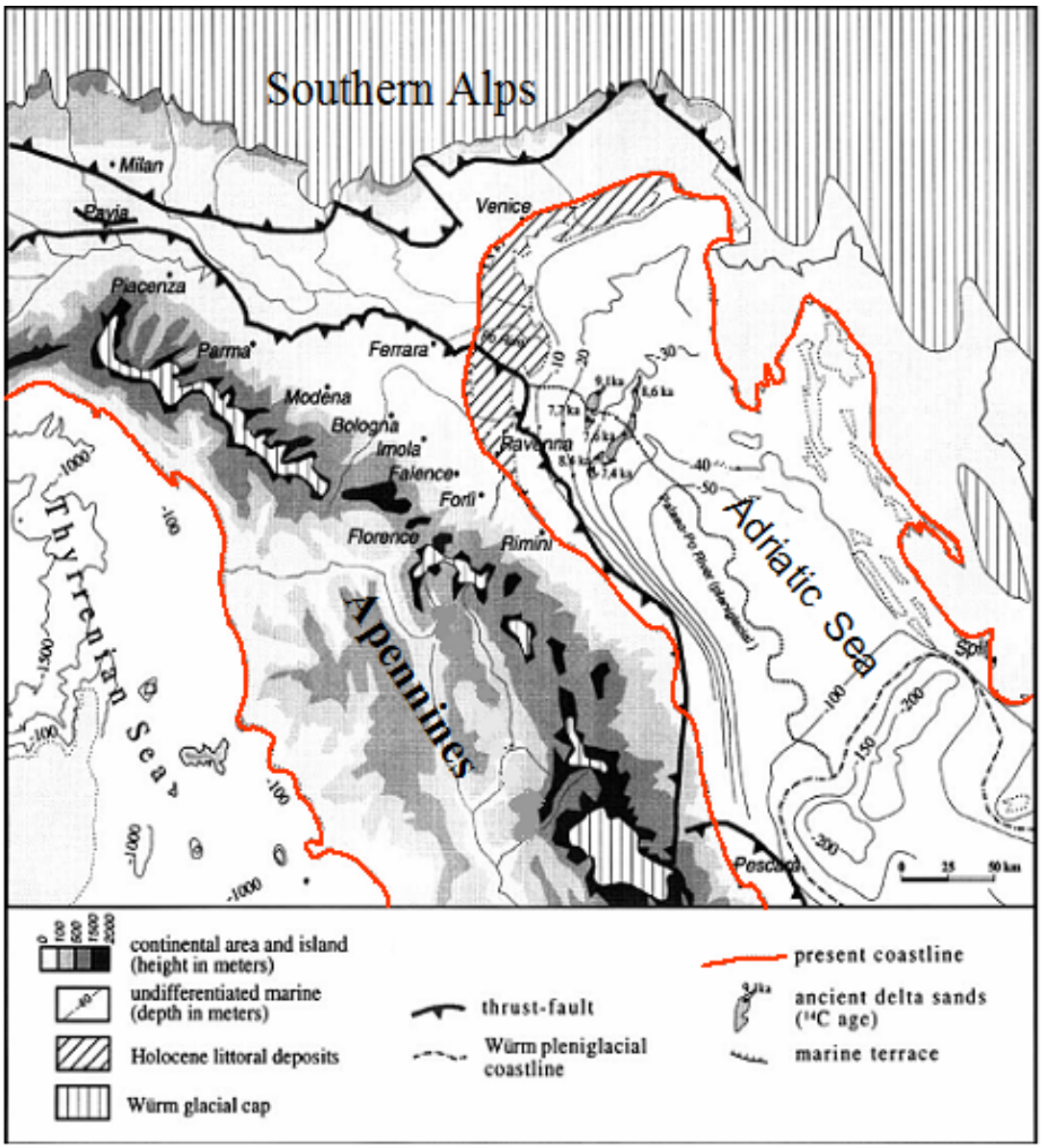

Figure 2-2: Schematic paleo-geographic map of the northern and central Italy; simplified structural map of the Adriatic-Apulian foreland basin (Farabegoli et al. 2004).

2.3 Deglaciation and Sealevel Rise

The Adriatic Sea is a semi-enclosed basin that remained connected with the Atlantic Ocean during the Last Glacial Maximum (LGM) ~21 kyr BP. This implies that the eustatic sealevel curve should be applicable to the Adriatic Sea. The eustatic sealevel curve, since the LGM can be characterized by three principal features: (1) a minimum level of ca. 125 ± 5m below present day sealevel at the time of the LGM, (2) a nearly uniform rise from around 15 to 7 kyr BP of ca. 10m kyr^{-1} and (3) a constant level for the last 7000 years, Figure 2-3, (Fleming et al. 1998). Farabegoli et al. (2004) have compared several Holocene eustatic sealevel curves from different global shelves. Most of the curves had

a similar trend with the report of Fleming, that the end of the last pleniglacial episode was about 17 kyr BP followed by a very rapid sealevel rise and then a fairly constant level to the present day condition. In literature (Farabegoli et al. 2004 and Storms et al. 2008) it has been reported that the relative sealevel history of the Adriatic Sea is consistent with the eustatic sealevel curve. During the Late Pleistocene to Holocene (between ca. 17 and 5.5 kyr BP), the Adriatic Sea has risen and a wide portion of the northern and central Adriatic alluvial plain of the glacial time was progressively drowned, and the shelf area of the Adriatic has increased eight-fold. The Adriatic Sea attained the present highstand sealevel around ca. 5.5 kyr BP, (Trincardi et al. 1994 and Cattaneo et al. 2003).

Storms et al. (2008) had adopted the uncorrected eustatic sealevel curve as a proxy of the relative sealevel to the Adriatic Sea. The authors indicated that the average rate of transgression on the coast was 28 mm yr^{-1}, between 120m and 26m isobath, corresponding to the inferred coastline positions respectively about 19 kyr BP (during the LGM) and 9 kyr BP, Figure 2-3. The rate of transgression was even higher during the two melt-water pulses. The coastline has shifted about 300 km north-westwards over the low gradient, flat marine bottom shelf at an average rate of about 300m yr^{-1}. About 5.5 kyr BP, the maximum flooding level of the Holocene transgression was 2 to 15 km upward of the present coastline, and more than 50 km upward of the Po delta. The sealevel curve of Storms et al. (2008) comprises most of the factors of sealevel history and is reliable with the eustatic sealevel curves of Fleming et al. (1998) and Farabegoli et al. (2004). This curve is considered as a realistic sealevel for the Adriatic basin simulation.

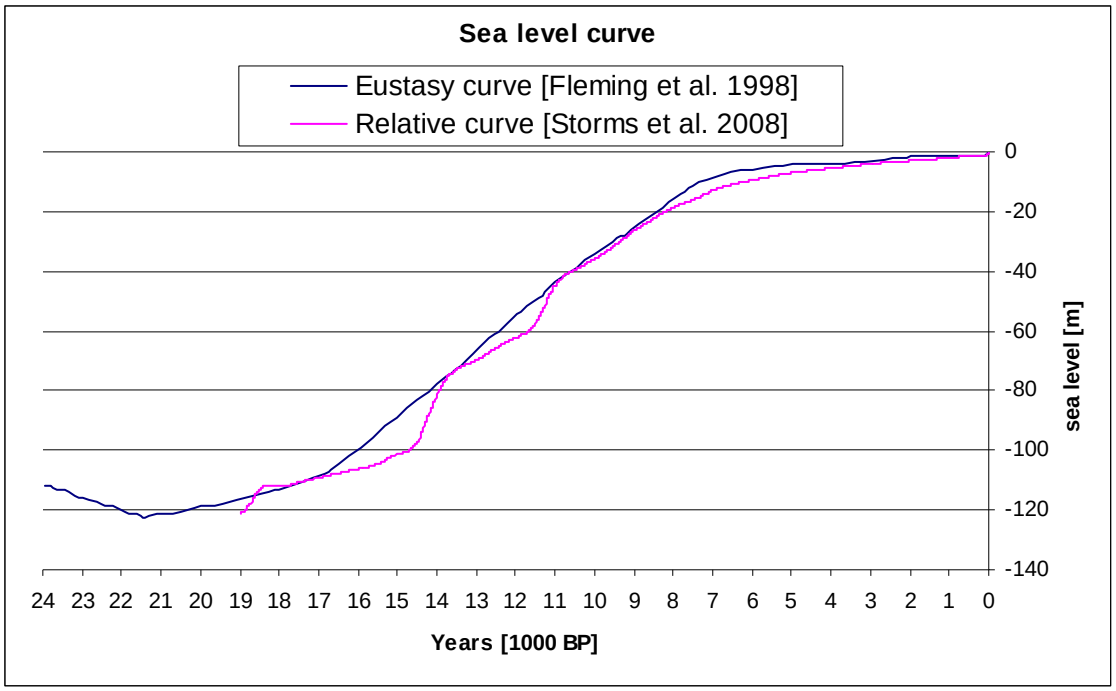

Figure 2-3: Eustasy sealevel curve and Relative sealevel of the Adriatic Sea.

2.4 Sediment Sources and Fluvial Discharges

During the late Quaternary, the Adriatic basin was filled with sediments mainly from the northwest in an axial direction favoured by the high uplift rates of the Apennines. The Adriatic sediment source is characterized by uneven distribution in which the major fluvial entry points are delivered from the Alpine in the north and Apennines in the west. The contribution of sediment from east, from the Croatian margin, is negligible since shore-parallel structural traps characterize this area, and very short and small rivers drain the extensively-karstified carbonate rocks, (Cattaneo et al. 2003). Thought many authors have subdivided the Adriatic drainage basin according to their research focus and interests, the northern and western Adriatic drainage can be subdivided broadly into four main drainage regions of the eastern Alpine rivers, the Po River, and the eastern Apennine catchments north and south of the Gargano promontory, (Cattaneo et al. 2003).

Brommer (2009) has subdivided the drainage area of the Adriatic basin into seven groups of river-basins analogous to represent different types of sediment source areas. The author used QRT and HydroTrend models which were designed to predict liquid and solid discharges of the fluvial drainage basins over the last 19,000 years. By modelling a representative source river for each area, they estimated total sediment supplied from each source area. The Alpine Rivers, the Po River and the Apennine Rivers were estimated to discharge respectively about 13000, 5000 and 3250 [$Mm^3\ yr^{-1}$]. The total solid sediment discharges of the Alpine and the Apennine Rivers were almost equivalent and supplied about 10Mt yr^{-1}, while the Po River had a supply of 31Mt yr^{-1}. The results showed that the sediment supply from the Po River and the eastern Alpine basins have been fluctuating strongly between 19 kyr BP and 12.5 kyr BP, caused by the deglaciation of the eastern Alpine. From 12.5 kyr BP to present, sediment discharge from these two basins remained more or less constant. A sudden decrease of sediment discharge of the Po River to ~15Mt yr^{-1} was observed since the 16^{th} century, attributable to the human impact in the river basin that had instigated trapping of sediments. Sediment supply of the non-glaciated Apennine basins remained more or less the same throughout the entire 19,000 years, (Brommer 2009).

Cattaneo et al. (2003) have estimated the present day sediment supply to the central Adriatic basin. The Po River has contributed about 15Mt yr^{-1}, while the Apennine rivers, north of the Gargano Promontory, added a total of ~32Mt yr^{-1}. The eastern Alpine rivers added only 3Mt yr^{-1} and the rivers south of the Gargano promontory were as low as 1.5Mt yr^{-1}. This low value of the southern river is due to combined effects of the relatively low gradients, karstified outcrops of the Mesozoic carbonates and a reduced precipitation relative to the northern areas. During the flood events of the Po River, liquid discharge on a daily-averaged of $8*10^9\ m^3\ s^{-1}$ has been reported, (Cattaneo et al. 2003). From the Pontelagoscuro station (50 km upstream of Po delta), historical annual mean records of the Po River shows a discharge of an average 1480 $m^3\ s^{-1}$ with a total sediment flux of 568 kg s^{-1} (18 Mt yr^{-1}). The concentration of the suspended load

sediment was recorded about 336 mg l^{-1}. An average monthly discharge concentration was about 500 mg l^{-1}, while during flood conditions, the monthly discharge averages between 3100 to 4350 mg l^{-1}. The sedimentation rate was estimated to be around 10 $Mm^3\ yr^{-1}$ with a sediment yield of 214 t $km^{-2}yr^{-1}$, (Syvitski et al. 2005 and Correggiari et al. 2005).

According to Syvitski et al. (2007), the Po River has an annual discharge of 1525 m^3s^{-1} as measured at Pontelagoscuro station. At this station, base-flow conditions were reported typically in the range of 700-800 $m^3\ s^{-1}$. Using the HydroTrend model, they suggested that the Po flood carried sediments between 18 and 42 Mt yr^{-1}. When a reduction of the sediment yield over the 20th century and trapping effects across the delta were considered, the model showed that the load was further lowered to a range between 7.5 and 18 Mt. They also analyzed sediment supply for five central Apennine rivers. The sediment load of each river was estimated between 0.4 and 1.3 Mt yr^{-1}. Based on ART model, the report also illustrated the northern Alpine rivers have been contributed 8 Mt yr^{-1}, the Po basin added another 13 Mt yr^{-1}, and the Apennine rivers contributed a total of 22 Mt yr^{-1}. These totals to a load of about 43 Mt yr^{-1} have been supplied to the Adriatic basin. Harris et al. (2008) have studied the freshwater inflows using combination of daily measured (from September 2002 through June 2003) and climatologically estimated data. Based on the model, the Po River had discharged about 15.6 Mt of sediment, while the Apennine Rivers delivered additional 28.9 Mt sediments in the specified time.

2.5 Hydrodynamic Conditions and Transportation Pattern

The Adriatic Sea is characterized by a microtidal regime and is dominated by a cyclonic anti-clockwise circulation, driven by a thermohaline and wind forced current called the *Western Adriatic Coastal Current (WACC)*. The semi-enclosed setting of the basin, the position of rivers input, the winter cooling of the northern part of the basin and the constraints of the Otranto sill (southern end of the basin) contribute to the formation of dense water in the north, and forces the outflow along the western flank of the basin, (Paschini et al. 1993 and Cattaneo et al. 2003). The main factors for the Adriatic hydrodynamics can be summarized into three main components. These are: (1) the river forcing about 5700 m^3s^{-1} fresh water input (more than half of which enters the northern Adriatic) causes heat loss and gains low-saline water; (2) the wind forcing on the water surface, produces deep-water masses and seasonal changes in circulation; (3) the Otranto channel forcing (reinforced by southeast Scirocco wind) balances the effects of freshwater discharge and the northern cooling by supplying a warm and salty water. The water exchange from the Mediterranean Sea in the south generates large-scale water current that flows northward along the eastern coast and southward along the western coast. This boundary intensified WACC is highly strengthened by seasonal wind storms. Two prevalent storm patterns exist in the Adriatic basin, called the Bora and the Scirocco winds. During winter, the cold Bora wind blows from the northeast and causes a down-welling, favourable currents along the western Adriatic coast. While during summer, the warmer Scirocco wind comes from the southeast and causes an upwelling

anti-cyclonic current along the western Adriatic coast. The Bora wind events enhance the WACC and cause a cyclonic gyre in the central and the northern Adriatic shelf while a small anti-cyclonic gyre is formed south of the Po region, (Paschini et al. 1993, Artegiani et al. 1997, Cattaneo et al. 2003 and Fain et al. 2007).

Even though the strong wind-storm events generate short-term circulation features that can enhance or override the general cyclonic gyre, the dominant cyclonic circulation (WACC) traps the fresh-fluvial water and the sediments southward along the western side of the basin. The southward current is mostly approaching 0.2 ms^{-1}, and is fastest in the southern Apennine region, (Fain et al. 2007). The strong southward transport creates a conveyor belt of sediment starting at the Po River and ending at the Gargano Peninsula which has the largest accumulation rate in the Apennine region, about 1 cm yr^{-1}, (Poulain, 2001, and Brommer et al. 2009). Combined effects of waves and currents on the western shelf of the basin have been assessed. The shallow surface wave-climate is characterized by a mean wave height of ~1.5 m and a maximum average wave height record of ~4.5 m. It has a wave period of 4 to 8 seconds and the velocity at the near-bottom wave boundary layer reaches to ~40 cm s^{-1}. Significant wave height frequency distribution was measured around the Ancona shelf during the winter Bora wind events 2000-2004 periods, and is shown in Figure 2-4, (Wang et al. 2007 and Harris et al. 2008). The data depict more than 80% of the wave height records were less than 3m.

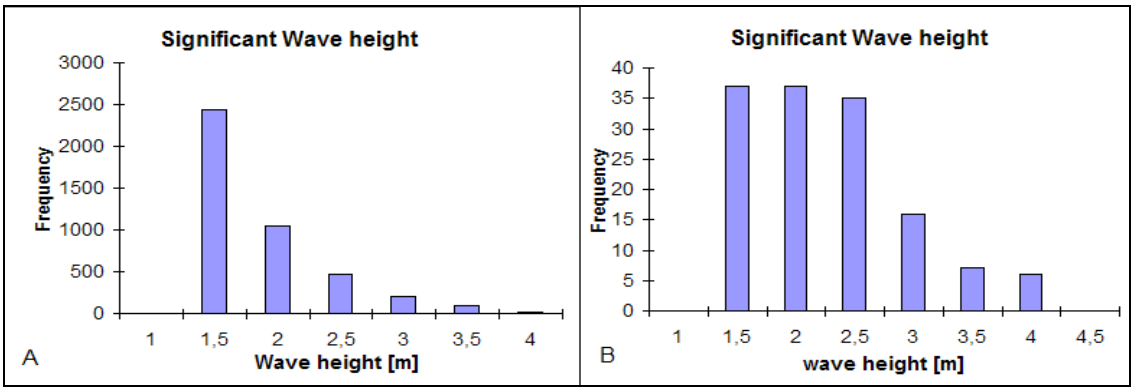

Figure 2-4: Significant Wave height frequency measurements at Ancona shelf: A) Harris et al. 2008, B) Wang et al. 2007

During the winter of 2002 through 2003, Harris et al. (2008) have calculated the sediment transport conditions in the Adriatic western shelf. The model showed the transportation mechanism was dominated by three types of mobile sediment sources; namely seabed sand fractions that settle at 10 mm s^{-1}; fine grained deposits that behave as a single grain with slow-settling rate of 0.1 mm s^{-1} and flocculated sediments that settle at 1 mm s^{-1}. The latter two were estimated to form roughly 90% of the supplied sediments. The authors also estimated sediment flux along the Apennine margin. Inshore of the 40m isobath, the longshore component dominates the flow pattern with mean current velocities of 0.04–0.06 m s^{-1}, and the cross-shelf current component was less than 0.01 m s^{-1}. The net erosion in the shelf area accounted for 6.7 Mt of bed

material north of the Gargano Promontory. Most of the eroded deposits were fine sediments, which were more easily mobilized than the sand fractions. The fine deposits were eroded above the 40m isobath from the northern shelf (areas north of the Po Delta and north of the Ancona) and above the 20m isobath from the central shelf (areas south of the Ancona). The sand deposits were eroded from all areas shallower than the 20m isobath. These erosional patterns seem to reflect adjustments of the assumed initial seafloor surface sediments to the hydrodynamic conditions of the basin (Harris et al. 2008). To evaluate the near-shore sediment transport processes, Fain et al. (2007) have deployed instruments on the Po subaqueous delta and on the Pescara River shelf (one of the largest Apennine Rivers) along the 12m isobath. Throughout the assessment period, the net sediment flux records were relatively higher along the southward longshore current, which was associated with the Bora wind. Current driven near bed velocities were about 0.1 to 0.15 m s^{-1}, which was sufficient enough for sediment re-suspension to occur. The authors also assessed the wave height frequencies on the shelf and the values were greater during the winter months, with a maximum significant wave height of 2.9m at 12m water depth and 4.2m at 55m water depth. On average, 10% of the shallow shelf recorded wave heights had exceeded 1.5 m. Fox et al. (2004) have also assessed the settling velocity versus grain size fractions on the Po delta. The settling velocities were in a range of 0.08 to 8 mm s^{-1} with a mean value of 1.2 mm s^{-1}. The values were associated with the concentrations of the flocculating materials delivered to the delta. In contrast, the Apennine sediments appear to consist of less easily flocculated material with lower settling velocities as observed offshore of the Pescara River, (Mikkelsen et al. 2007).

2.6 Grain-size Distribution and Spatial Dispersal Pattern

Brommer (2009) have investigated 87 prodelta cores and 22 riverbed sediment samples. The grain size distributions (GSDs) of the samples were 80 to 90% clay and silt-sized particles, barring some exception of the river mouths samples. The river mouth samples were mainly an admixture of fine to very fine sand particles. The GSDs of nearly all of the samples also show a bimodal distribution within the fine sediments comprising a population of clay to very fine silt (cohesive < 20 µm), and a population of medium to coarse silt (cohesionless 20 – 63 µm). The basin scale spatial dispersal pattern of the cohesive and cohesionless sediments on the Northern Adriatic shelf is displayed on Figure 2-5, (Brommer 2009). The maps show a fining trend both longshore and cross-shore of the western Adriatic coast. Figure B, presents the spatial distribution of mean grain size of the sortable (cohesionless) coarse silt fraction, and near the Po Delta area on average it is coarser than the surface sediments in the central Apennine Region.

Milligan et al. (2007) have also collected box-core samples on girded-stations offshore of the Po Delta to observe the evolution and transportation of sediments from flood event of 2000. From the estimated floc limit (~20 µm), the fine sediments of 5-18 µm in size act as cohesive material and have been transported and deposited predominantly as flocculation. The sediments coarser than 18 µm were transported and deposited as a

single grain. The floc deposition accounted for up to 75% of the total mass found in the seabed-surface sediments at the stations located below the plume.

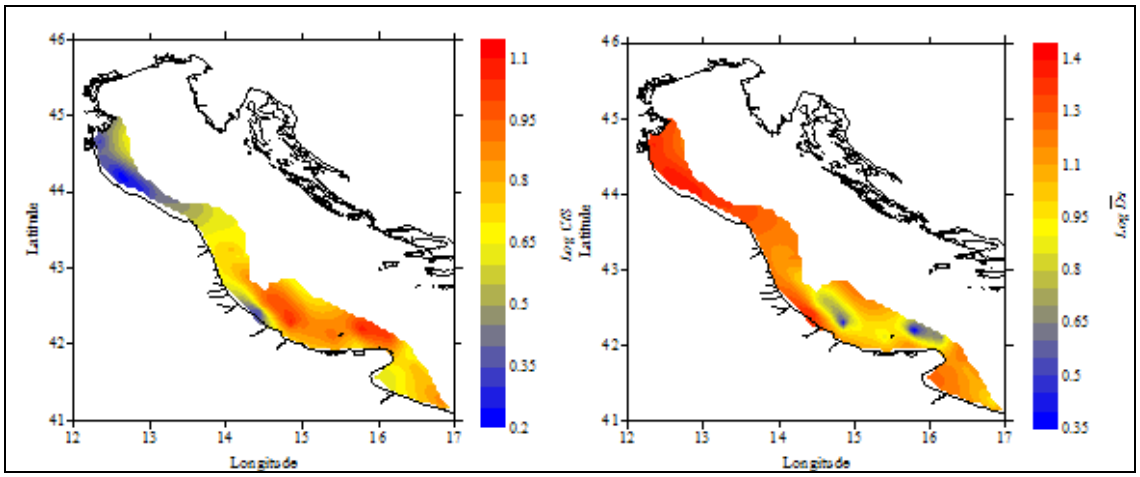

Figure 2-5: Grain size distribution maps; A) Log C/S (*C* fraction: < 20 µm; *S* fraction: 20-63 µm); B) Log plot of S-fraction; Brommer (2009).

From the grain size distribution assessments, the Adriatic shelf deposits can be generally described as containing about 80% less than coarse silt size [75% cohesive ~18 µm; 25% non-cohesive 18 -63 µm] and the remaining 20% are very fine to fine sand particles (>63 µm).

2.7 Sedimentation Rates and Preserved Deposits

The Northern Adriatic Basin is a well-documented, closed basin where the paleo-sediment masses can be reconstructed from time-averaged, basin wide mass accumulation rates. Frignani et al. (2005) have estimated the sediment budgets on the western Adriatic continental shelf. The authors have measured the mass accumulation rates from more than 100 sediment core activity–depth profiles of ^{210}Pb, collected by many researchers over the last 20 years. Depending on the lithological composition of the sediment sources and the orientation of the coastline, the authors have estimated the river sediment supplies and accumulation rates. The estimated rates encompass a wide range of values between 0.03 to 6.62 g cm^{-2} yr^{-1} and average value of 0.43g cm^{-2}yr^{-1}. The highest values were recorded in the prodeltas of the Isonzo and the Po rivers. The total estimated sediment flux along this continental shelf was 46 Mt yr^{-1}, with a mass accumulation rate of 42 Mt yr^{-1}. The sediment budget of the Adriatic shelf reveals about 10% of the fluvial load might be delivered to the southern Adriatic basin and/or to the Mediterranean Sea, (Frignani et al. 2005).

Studies have also been done on parts of the subaqueous delta which have no direct fluvial input. Around the Gargano promontory, Cattaneo et al. (2003) have estimated the sediment accumulation rate of the last century deposits on a subaqueous delta. The authors determined the volumes and the deposition rates from core sub-samples of ^{210}Pb. The estimated volume was about 27 Gm^3, which is about 1/7th of the total volume

of the Late-Holocene mud wedge, (~182 Gm^3). The core samples further showed that sedimentation rate, on a century time scale, was between 0.33 cm yr^{-1} and 0.57 cm yr^{-1} with a highest record on the foreset of the subaqueous delta. Brommer et al. (2009) have estimated the sediment masses of five basin-wide lithosomes of the Late Quaternary deposits (19 kyrs) from high-resolution seismic maps, porosity profiles, and radiocarbon dating (^{14}C). The estimated sediment masses are summarized in Table 2-1. Deposits of 5.5 kyr BP to present day (Highstand Systems Tracts) and 19 to 5.5 kyr BP (Transgressive Systems Tracts) comprise total mean sediment masses of 254 Gt and 486 Gt, respectively. The Mid Adriatic Deep (MAD) deposits contribute about 15 % of the total sediment mass of the TST units, and only 2% to the total sediment mass of the HST units. Basin-wide sedimentation rate has been also estimated for the five lithosomes and is also summarized with their uncertainties in Table 2-2. The net basin wide sedimentation rate was roughly 39±3 Mt yr^{-1}.

Table 2-1: Sediment masses M_σ (all estimates (μ) and standard deviations (σ) in Gt). Symbol "--" indicates mass is negligible.

Lithosome	Delta		Shelf		MAD		Total	
	μ	σ	M	σ	μ	σ	μ	σ
HST-2	2	1	17	2	-	-	18	2
HST-1	14	7	222	26	4	1	236	28
TST-3	5	2	177	27	30	12	212	40
TST-2	-	-	98	8	19	8	116	16
TST-1	-	-	37	4	121	18	158	22

Table 2-2: Estimated ages of bounding surfaces, σ [kyr], duration of time slices τ [kyr], and net accumulation rates S_σ [Gt kyr^{-1}] from stratigraphic record.

Bounding surface	Lithosome	σ	$\delta\sigma$	τ	$\delta\tau$	S_σ	δS_σ
HST-2/HST-1	HST-2	0.4	0.04	0.4	0.04	45	7
HST-1/TST-3 (MFS)	HST-1	5.5	0.17	5.1	0.17	46	6
TST-3/TST-2	TST-3	11.3	0.34	5.8	0.38	37	7
TST-2/TST-1	TST-2	14.8	0.44	3.5	0.56	33	7
TST-1/LST (MRS)	TST-1	19	0.57	4.2	0.72	38	8

2.8 Adriatic Stratigraphy

Four basin-wide stratigraphic surfaces have been recognized by ^{14}C age dating and in accordance with this established surfaces, two Systems Tracts were identified, (Correggiari et al. 2001 and Brommer et al. 2009). The recent sediments that were deposited during the highstand sealevel have been described as Highstand Systems Tracts (HST) and are subdivided into an upper unit (HST-2; 0.4 kyr BP to present) and a lower unit (HST-1: 5.5 – 0.4 kyr BP). These two units are bounded by conformable surfaces, and the lowermost surface represents the maximum flooding surface (MFS). These units were developed on the north-western shallow shelf of the Adriatic basin. The Transgressive Systems Tracts (TST), which contains the record of abrupt deglacial sealevel rise, comprises three lithosomes. These are the upper unit (TST-3; 11.3-5.5 kyr

BP), the middle unit (TST-2; 14.8-11.3 kyr BP), and the lower unit (TST-1; 19.0-14.8 kyr BP). These units are separated by unconformable ravinement surfaces with the exception of the TST-1 unit, which is bounded locally by the maximum regressive surface (MRS) in places where this surface has not been cut by the lowermost ravinement surface, (Trincardi et al. 1994, Correggiari et al. 2001 and Brommer et al. 2009).

Brommer et al. (2009) have reported stochastically reconstructed stratigraphic maps from the basin wide estimated sediment masses. The sediment volumes of the shelf units (TST-3 and HST) were estimated from stratigraphic profiles, while the sediments offshore of the shelf and deposits in the MAD (TST-2, TST-3, and HST-1) were estimated from accumulation rates measured from sediment cores. The reconstructed stratigraphic maps of the Highstand and the Transgression Systems Tracts are displayed separately in Figure 2-6 and Figure 2-7.

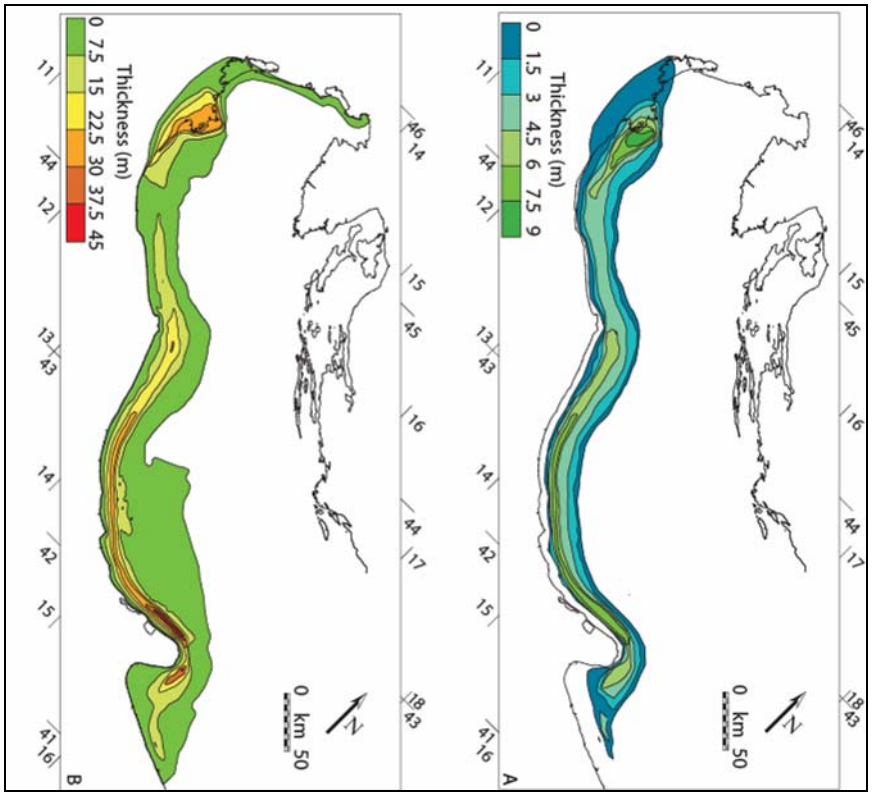

Figure 2-6: Isopach maps [m] of the HST units: A) HST-2 and B) HST-1; Brommer et al. (2009).

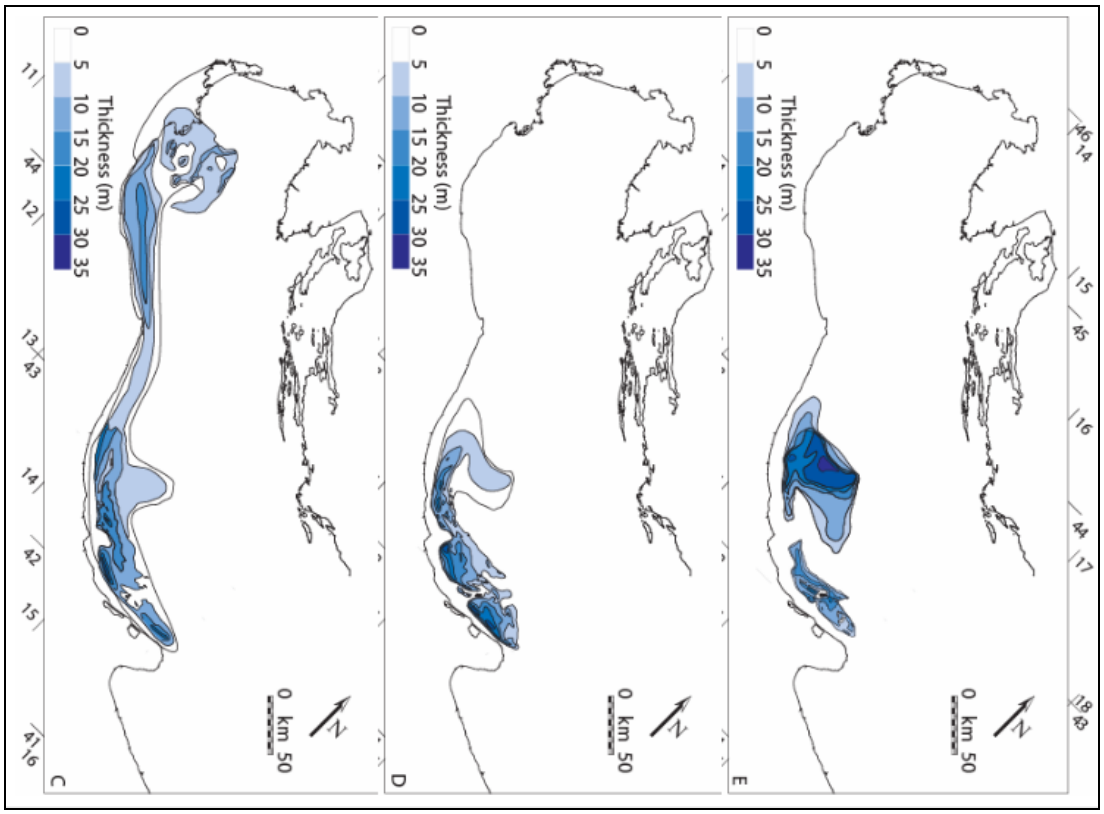

Figure 2-7: Isopach maps [m] of the TST units: C) TST-3, D) TST-2, and E) TST-1; Brommer et al. (2009).

Chapter 3: The Numerical Model

This chapter summarizes the 3D basin scale numerical model which was used to simulate the morphological and stratigraphical development of the Adriatic basin. The model comprises fluvial and marine system algorithms, which are designed to simulate the sediment distribution and stratigraphic response of a continental shelf in a high energetic hydrodynamic activity subjected to waves and currents. Under sufficiently energetic conditions, sediment previously deposited on the shelf may be resuspended and transported. This condition effectively segregates the fine grain classes from the coarse fractions that hug near the coastline. An algorithm was developed to represent the effect of waves and currents on marine clastic sedimentation. Longer time scale (one year time-averaged) simulation was chosen to realize the influence of a large-scale continental fluid transport, and basin currents and waves for sediment distribution in a shelf. Here presented is a summary of theoretical algorithm developments which are adopted in the model application. It is taken from the reports of Dalman and Weltje 2008 and Dalman (2009). For further details, it is advisable to refer the original literature of the authors.

3.1 Continental Clastic Sediments and Network Systems

The continental clastic sedimentary system is characterized by two algorithms. Fluvial processes and stratigraphy are represented by sub-grid parameterization for application in the large scale basin filling model, (Dalman and Weltje 2008). Sub-grid sediment transport and channelization are derived from physical equations, capable of detailed representations of avulsions and bifurcations. The channel network is kept constant until it becomes unstable or too little discharge is received to keep the channel open. Mean flow velocity along the channel was computed by the Darcy-Weisbach equation and sediment transports are determined from shear velocity. The bed-load transport rates are determined by equation (1); a modified Bagnold bed-load transport Equation.

$$i_b = \frac{c}{\tan \alpha}(U_* - U_{*_c})(\tau_0 - \tau_c) \quad \text{..... (1)}$$

Where i_b is the bed-load sediment transport, U_* and U_{*_c} the effective and critical shear velocity; τ_0 and τ_c are respectively effective and critical shear stress. Coefficient ($c/tan\ \alpha$) represents bed roughness and dynamic friction, whose value is empirically derived as 10. The concentration profile and transportation rate of the suspended load are derived using the Rouse Equation.

The stability of channels network is evaluated each time step by a balance ratio between the sediment load and the transport capacity. Incising channels are unconditionally stable. Channels that are aggrading and in equilibrium (at grade) are conditionally stable, which are subjected to avulsion and bifurcation. Different events can trigger avulsion that initiates crevasse. Dalman (2009) has discussed the channel network controlling factors, and the main controlling factors of the process are the progressive increase

cross-valley slope and, to a lesser extent, the amount of the suspended sediment in the main channel. The super elevation of the channel above the surrounding floodplain is parameterized and allows gradual channel aggradation. The avulsion process in the model is then described as a self-stabilizing process, governed by a balance between the ratio of sediment load and the transport capacity. If the sediment load is greater than the transport capacity, the crevasse is unstable and will heal, otherwise the crevasse will incise if the transport capacity is greater than the sediment load. This divergent distributary system is modelled by a diffusive routing algorithm in which a fluid is routed to all lower-laying neighbouring cells in quantities linearly-proportional to the slope. This diffusive method with some boundary condition assumptions has captured the essence of the drainage network evolution and allows the channel pattern to be preserved. A stochastic realisation of sub-grid alluvial stratigraphy in the proximal reaches of the fluvial domain is displayed in Figure 3-1.

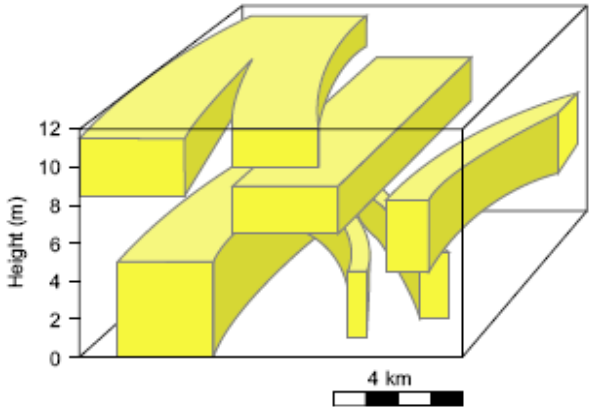

Figure 3-1: A realisation of alluvial sub-grid stratigraphy in the upper reaches of the fluvial system; (coarse-grained channel belt deposits are visualised in yellow, overbank fines are invisible); (Dalman and Weltje 2008).

This channel network model allows a realistic input and more importantly spatial and temporal changes of the liquid and solid discharge entering the marine domain, which incorporates autogenic lobe switching due to avulsions near the apex of the delta.

3.2 Hydrodynamics of the Marine System

The hydrodynamic process of the marine system focuses on clastic sediment dynamics and depositions. In the model, it is represented by individual processes of: *river plume and oceanic current* in one combined algorithm; and *wave generation* represented in separate algorithms.

3.2.1 River Plumes and Large Scale Oceanic Currents

The hydrodynamic flow of currents and plumes are simulated using one integrated steady-state potential flow routine, which is representative for a geologic time scales. This allows to calculate the deposition of sediments from the river plume and the longshore transportation of the resuspendable shelf deposits. The general Laplace

equation (2) for potential flow in 2-D form is used to represent the current and plume flows.

$$\frac{\partial^2\phi}{\partial x^2}+\frac{\partial^2\phi}{\partial y^2}=0 \qquad v_x=\frac{\partial\phi}{\partial x} \qquad v_y=\frac{\partial\phi}{\partial y} \qquad \text{..... (2)}$$

Where ϕ is the velocity potential, V_x and V_y are the velocity components in the x and y directions (either of plum or current velocities). The input for the flow field is provided by supplying the velocity at the grid boundaries. The plumes entering the marine domain are dynamically integrated by automatically assigning an inflow point with the channel velocity and direction of flow at the appropriate grid cell. Depending on grain size distribution, the coarse sediment loads entering the marine basin under hydrodynamically inactive periods is dumped within the first tens of kilometres of the coast. Additionally, the wave-current interaction may rework a significant proportion of the fine-grained fractions deposited by the plume.

3.2.2 Wave Generation

The waves have different characteristic change of their height, length and orbital motion in various marine sub-environments. Figure 3-2 illustrates the principle of propagation and consequent shoaling of waves at different water depth, and in the model, each marine gridcell is assigned to one of these three sub-environments (Dalman 2009).

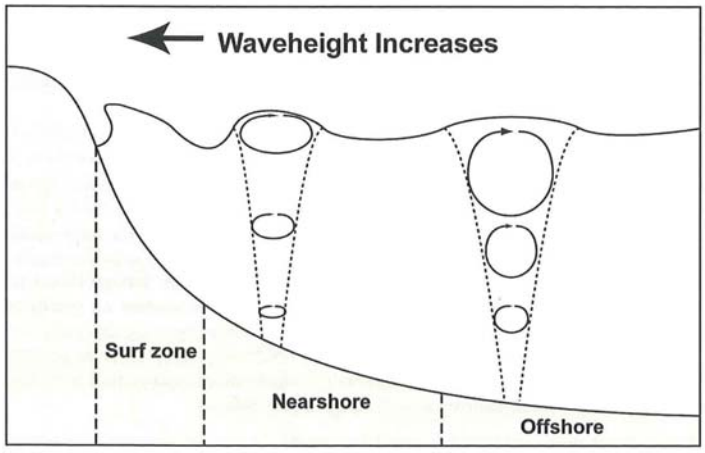

Figure 3-2: Cartoon of the changes in wave height, length and orbital motions in different zones. Each marine gridcell is assigned to one of these three sub-environments, (Dalman 2009).

For an effective use of wave simulations, once-a-year storm induced deep sea wave height is provided as an input in the model. As wave height alone is not sufficient for the simulation purpose, the linear Airy wave theory is also used to simulate a fully developed wave algorithm. At shallower area, the wave parameters due to shoaling effect are expressed with respect to a deep water wave. The shallow and deep water relationships of the wave parameters are summarized in the equations (3):

$$C = \frac{gT}{2\pi}\tanh\left(\frac{2\pi h}{L}\right) \text{ at deep water } (h > L/2),\ C_{\infty} = \frac{gT}{2\pi}$$

$$L = \frac{gT^2}{2\pi}\tanh\left(\frac{2\pi h}{L}\right) \text{ at deep water } (h > L/2),\ L_{\infty} = \frac{gT^2}{2\pi} \quad \text{..... (3)}$$

$$H = H_{\infty}\left[\tanh(kh)\left(\frac{2k}{\sinh(2kh)}\right)\right]^{-1/2}$$

Where H is wave height, *C* is phase velocity [m/s], g is gravitation, T wave period [s], h water depth [m], L wave length [m] and (k=2π/L) is a wave number.

3.3 Integrated-Model Algorithms

The wave and the current fields were represented independently and must be combined to form a total flow field. They are modelled to interact through the sediments, which are dominantly characterized by the suspended load transport of the fine grain deposits.

3.3.1 Sediment mobilization

In the model, annual storm event and current induced resuspension and transportation algorithm is assumed. This assumption is valid in the marine process as the majority of sediments in the shelf are eroded during such events. It is modelled by finding the depth at which the bottom shear stress is equal to the critical shear stress. The critical shear stress τ_{cr}, which initiates the suspension transport, is given by equation (4):

$$\tau_{cr} = 0.64\rho W_s^2 \quad \text{..... (4)}$$

Where W_s is the settling velocity defined as a function of dynamic viscosity as well as fluid and sediment densities. The bottom shear stress can be determined under various conditions of wave influenced; current influenced and combined current-wave interaction. The combined effect is much complex and thus the wave only or the current only is used in the model when the velocity ratios are smaller than 0.01. This has a negligible error and allows less computation time. The most important of these is the wave-influenced condition given by equation (5):

$$\tau_b = 0.5\rho f_w u_b^2 \quad \text{..... (5)}$$

Where u_b is the maximum wave induced orbital velocity and f_w is wave friction factor. The current only condition, which is relatively slow and has much lower carrying capacity, was defined as a function of flow velocity of depth (z) above seabed using the von Karman-Prandtl of equation (6):

$$u_z = (u_{*c}/k)\ln(0.3z/2.5D) \quad \text{..... (6)}$$

Where u_{*c} is the total current shear velocity, *k* Von Karman constant=0.4, and *D* grain diameter[m]. The bottom shear stress for the steady currents with a current friction factor f_c is then calculated as equation (7):

$$\tau_b = 0.5\rho f_c u_z^2 \quad \text{..... (7)}$$

3.3.2 Marine sediment transportation and deposition

The suspended particulate matters (SPM) are temporarily kept in suspension and are dispersed due to the wave and the current motions. The model simulates the process by applying an explicit diffusion routine to the suspended particulate matter, excluding the sediment delivered from the rivers in the present time. The transport mechanism is represented by the current only algorithm, as the effective velocity vectors of the waves are mostly oriented to the cross-shore direction. The deposition rate of the SPM is estimated by a first order rate law (Syvitski 1988):

$$dI / dt = -\lambda I \quad \text{..... (11)}$$

Where *I* is the total mass of the SPM in the water column per area and λ is the removal rate. The remaining SPM after a time step are related to an earlier step by integrating *dt*.

$$I_{t+\Delta t} = I_t e^{-\lambda \Delta t} \quad \text{..... (12)}$$

The time step is calculated using the current flow velocity and the size of the grid-cells, thus allows the necessary time for the quantity of the SPM to move from one grid cell to other. It is realistic assumption that the simulation time step (once a year) is sufficiently large to allow all SPM to fall out of suspension. By repeatedly cycling through the entire model area, the simulation process continues until all the SPM is iteratively removed and gradually deposited. Most imperfections in the algorithms of the model are very small compared with the uncertainties of morphologic and stratigraphic boundary conditions of a basin in a geological time scale, (Dalman 2009).

Chapter 4: Sensitivity Test of the Model on a Synthetic Basin

The chapter deals with sensitivity tests of the initial and boundary conditions of the numerical model. The main objective of the test is to mimic comprehensive effects of the simulating factors on the sediments dispersal and depositional architecture in a basin. Moreover, the test provided a vital understanding on the application and usage of the model. The gradient and width of the shelf; wave height and current velocity of the marine domain; grain size fraction of a fluvial supply; and grain size characteristics of the substratum sediments are considered as calibration parameters of the model. During the experiment, each parameter has been simulated and interpreted independently in a rectangular constrained synthetic basin. This basin is a closed system which differs in the proximal and offshore shelf geometry. This setup was made so as to represent the semi-closed, rectangular and shallow Adriatic shelf. The basin substratum in all of the experiment was set to have resuspendable surface deposits of 1m thickness with 20% of coarse sediments. The models have been simulated for 1000 years with one experiment at a time. The setup of the experimental scenarios is summarized in Table 4-1. Finally, when each of the factors has been simulated and interpreted, a comprehensive multi-river system was simulated in experiment-6. During the interpretation, the deposited sediments mass were extracted from the initial bathymetry profile. These resulting sediment mass were then subtracted from the total fluvial supplied sediments to determine the cross-shore and longshore drifted proximal shelf deposits. These net deposits mass were considered as preserved shelf deposits under the hydrodynamic conditions, and were interpreted in the following sensitivity analysis as a preservation potential of the sediments on the proximal shelf of the synthetic basin.

Table 4-1: Experimental scenarios for sensitivity test of the model on synthetic basin.

Model input parameters	Experiments					
	Experm. -1	Experm. -2	Experm. -3	Experm. -4	Experm. -5	Experm. -6
Shelf gradient [degree]	0.007 to 0.12	0.029	0.029	0.029	0.029	0.029
Wave stabilized Shelf width [km]	40	10 to 120	40	40	40	40
Wave height [m]	4 to 4.5	4	2 to 5	4	4.3	4.2
Current velocity [m/s]	0.3	0.2	0.2	0.05 to 0.3	0.2	0.3
Fluvial fine grain size [%]	80	80	80	80	20 to 90	80
Substratum thickness [m]	1	1	1	1	1	1
Substratum coarse grain [%]	20	20	20	20	20	20

4.1 Experiment-1: Shelf Gradient Analysis

Gradients ranges from very shallow 0.0070 (0.5m in 4000m) through very steep gradient of 0.1150 (8m in 4000m) have been assessed during the experiment-1. Depositional thickness for all of the simulations was then interpreted to quantify the gradient response to sediment reworking and transportation process. For an illustration, the cross sections of very steep and shallow gradients are shown in Figure 4-1. The figure

reveals the shallow shelves were more sensitive to the hydrodynamic condition of the model. The sediments were transported offshore to ~30 km and a flat-topped deposit was formed. Sediments on a steep shelf were less affected by the marine conditions and were dispersed to an offshore direction, where they finally fallout to the shelf and forms a very thin deposits.

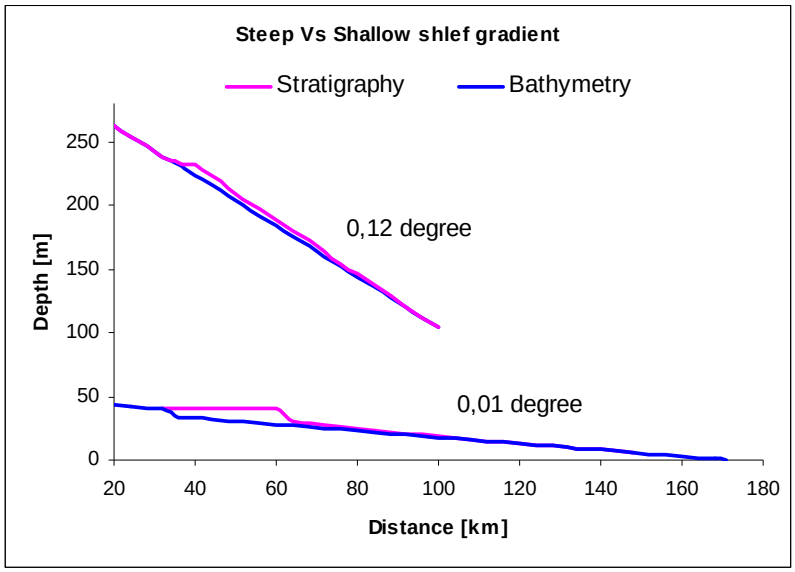

Figure 4-1: Cross-shore depositional profiles of steep and shallow shelf gradients.

Preserved deposits with thickness greater than 3 cm were assessed to determine the processes of sediment dispersion and deposition on the shelf. The depositional trend illustrates as the gradient increases steadily, sediments were dispersed to an offshore direction leaving small deltaic formation on the proximal part of the shelf. The lower gradient shelves have created a wide, reworked and relatively thicker deposits under the wave level. They have a preservation potential of ~50% on the equilibrium proximal part of the shelf. Figure 4-2 displays the preserved shelf sediments vs. the gradient of the shelves. Both longshore and cross-shore drifted sediments were also assessed and are illustrated in Figure 4-3. The gradient impacts on the transportation are represented by power-law equations. The results depict that longshore transportation effect is much more sensitive to the basin gradient than the cross-shore, though both decrease with increase of shelf gradient.

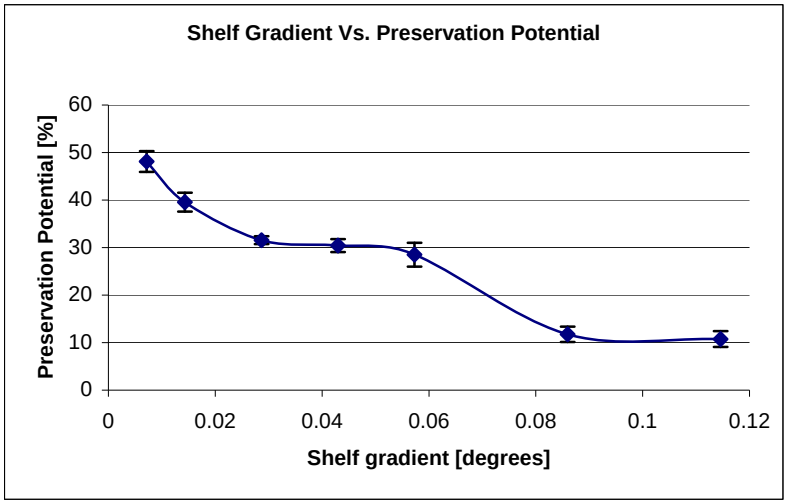

Figure 4-2: Gradient effect on preserved sediments with their STDEV.

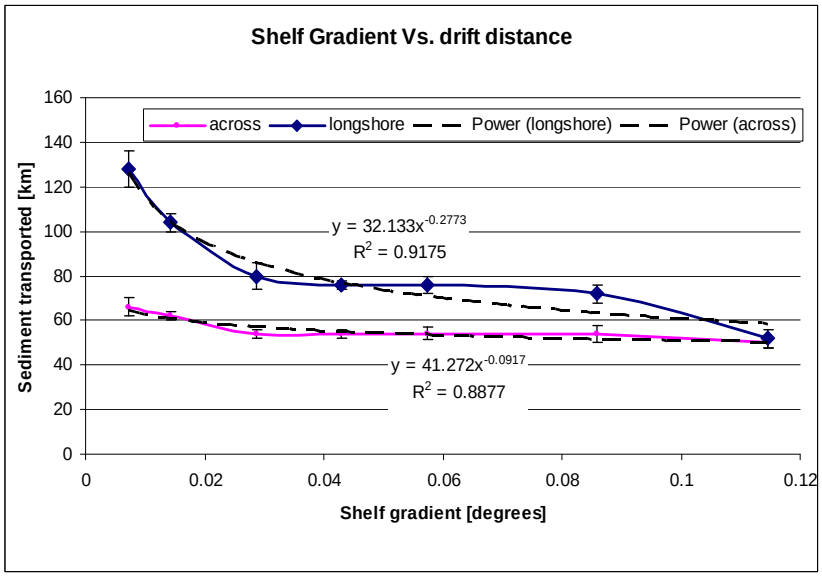

Figure 4-3: Shelf gradient and drift distance assessment with their STDEV.

4.2 Experiment-2: Shelf Width Analysis

In experiment-2, shelf width was tested; so as the hydrodynamic capacity for resuspension and transportation on a wider shelf can be traced. The relationship of a wave stabilized shelf width and its preservation potential are shown in Figure 4-4.

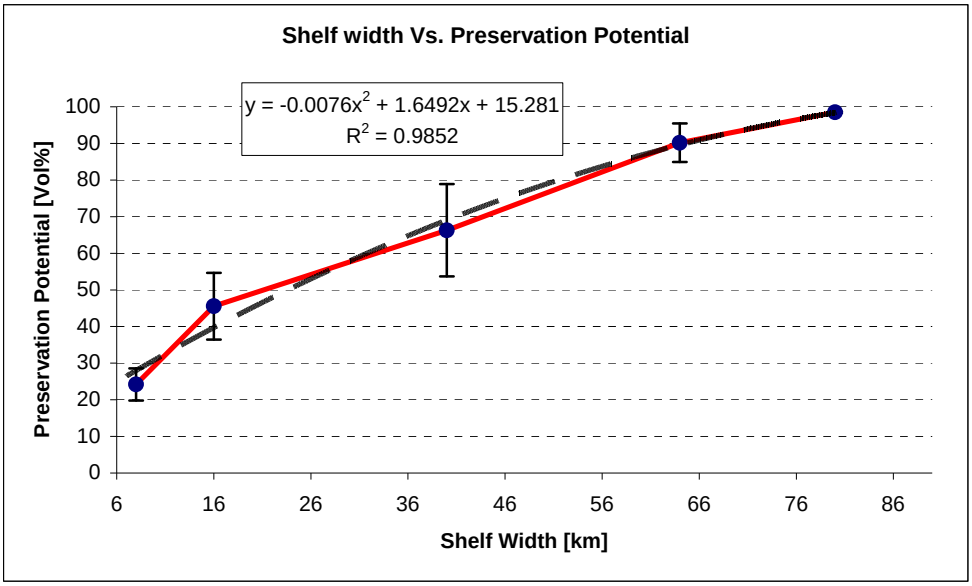

Figure 4-4: Shelf width and preserved shelf deposits, with their STDEV.

The figure displays the discharged and reworked sediments remain with in the stable part of the shelf in logical relationship to the increase of the shelf width. The assessment illustrated in every 1000m widening of the shelf, there was an additional 1.5% increase of preserved deposits. Assessment on a wider shelf indicated that sediments were reworking and are dispersed efficiently both longshore and cross-shore directions. The model also revealed a preservation potential of ~ 95% on the wider shelf, where the fine materials have transported as far offshore as 76 km.

4.3 Experiment-3: Wave Height Analysis

For wave height assessment, 2 to 5m deep sea wave heights with the parameters of experiment-3 were simulated. Preserved sediments along the wave stabilized shelf was assessed. Result of the routines elucidates wave heights of less than 4m have almost similar impact on sedimentation. More than 80% of the supplied materials have retained on the proximal area of the shelf, Figure 4-5. Figure 4-6 also illustrates the shelf geometry with the preserved proximal delta deposits. As the mean wave height increases above 4m, the amount of the sediments which were preserved at the shallow shelf decreased faster and an offshore transportation became prominent. Further increase of wave height, above 4.5m, has removed all the river supplied materials and has eroded the bathymetry surface sediments. This phenomenon is consistent with the wave base parameterization of the model which has a base depth of around 6m. The effect is illustrated by a decreasing (and negative) preservation potential in Figure 4-5, and in Figure 4-7(B) by an erosion of the proximal shelf and excessive sedimentation over far offshore on the deeper shelf. It also reveals that the subaqueous deposits have prograded relatively along the shore.

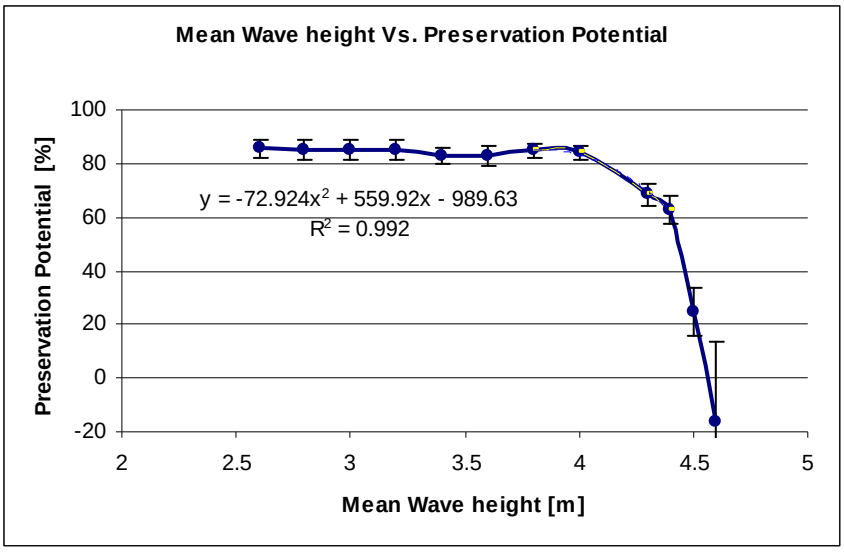

Figure 4-5: Effects of wave height on shelf deposits with their STDEV. The negative value indicates erosion of the substrate.

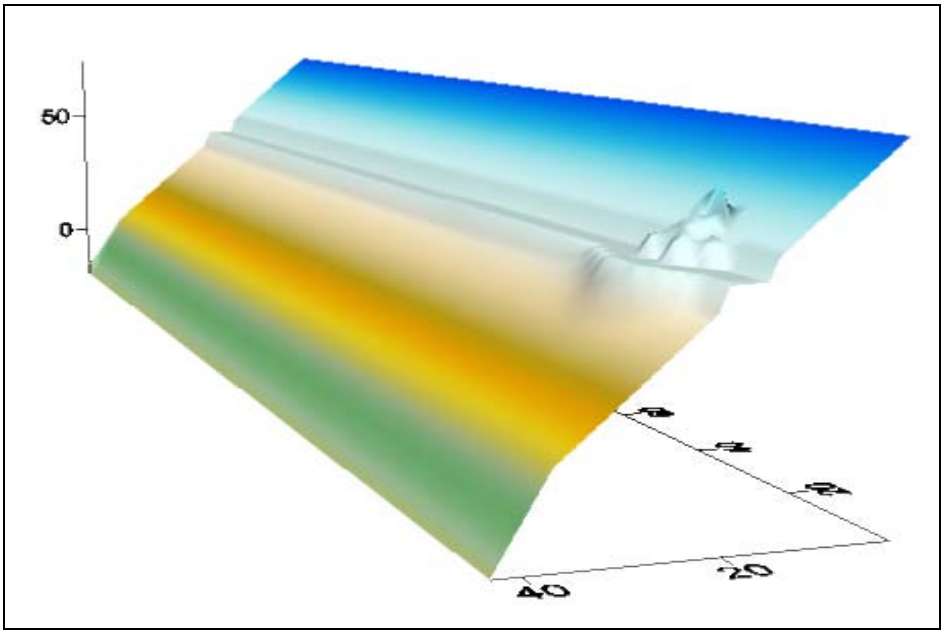

Figure 4-6: Shelf geometry with deltaic deposits; simulated at 4.2m wave height. [Scale 1 gridcell =4km]

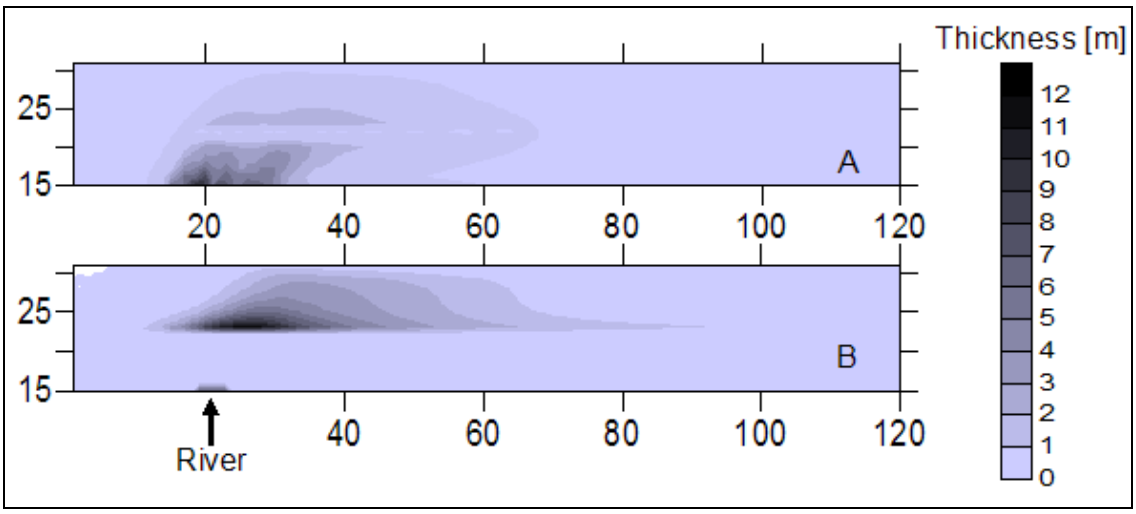

Figure 4-7: Wave effects on marine sediments: Isopach maps of A) less than 4m wave height; B) more than 4.3m wave height [Scale 1 gridcell =4km]

4.4 Experiment-4: Sea Current Velocity Analysis

In order to analyse current flux, velocity ranges of 0.05 ms^{-1} through 0.3 ms^{-1} were assessed in the experiment. Deposits thicker than 3cm were interpreted. Low current velocities (0.05 to 0.18 ms^{-1}) have illustrated a very narrow change of depositions (~70 to 72%) and the sediments were dispersed longshore for more than 140 km, Figure 4-8. When the velocity was increased to more than 0.2 ms^{-1}, the deltaic deposits decreased steadily; and the fine materials moved longshore further to more than 180 km. Isopach map of Figure 4-9 displays the morphological effects of the increased current velocity on the shelf deposits. At higher velocities, the shallow shelf deposits have longshore elongate morphology, while the deep marine deposits on the other hand have a consistent patchy morphology in all of the velocity ranges. These sediments have been transported by the wave action, which was constant in all of the scenarios. The analysis also confirmed that the current flux has much impact on the longshore transportation, and on average, an additional current increase of 0.025 ms^{-1} has increased the longshore dispersion further by ~7 km. In all of the high-velocity scenarios, patches of coastal deposits have also been interpreted at a longshore distance of 320 km (~ 80 gridcell size). These features could express the avulsion process of the model; possibly generated when the avulsion steered the river in the downstream direction of the general current field.

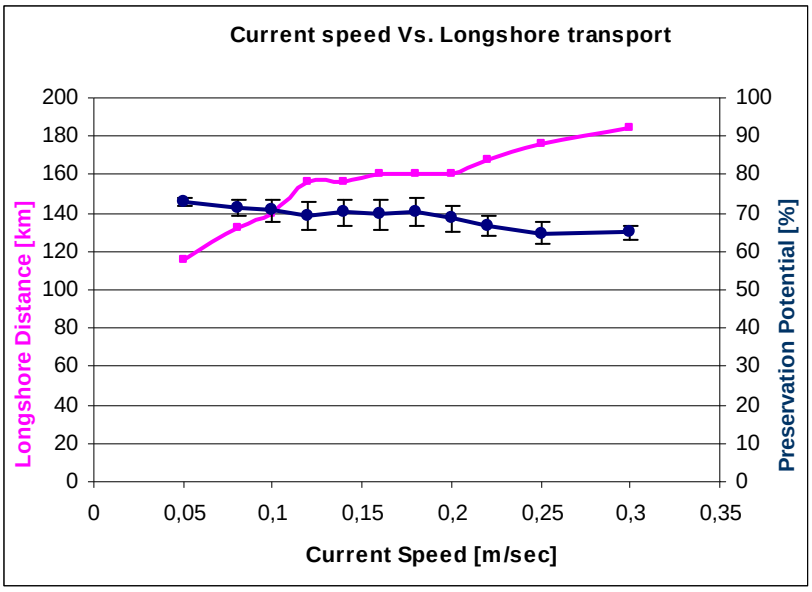

Figure 4-8: Current speed effects on cross-shore and alongshore sediment dispersals.

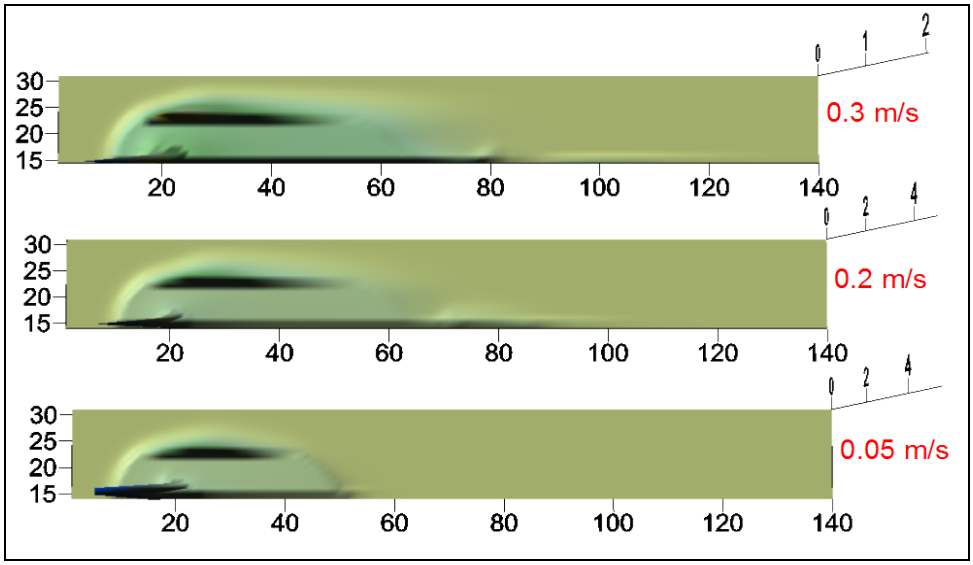

Figure 4-9: Current velocity effects on the morphology of marine sediments. [Scale 1 gridcell= 4km]

4.5 Experiment-5: Fluvial Grain Size Fraction Analysis

To mimic fluvial grain size impact on the morphology, a range of 5% to 95% of coarse grain sediments have been assessed. In the experiment, the finer domain was assumed to represent “clay and fine silt” sizes; and the coarse fractions represent “coarse silt to medium sand” deposits. Dispersed sediments of 2cm thickness have been interpreted for the analysis. The coarser fractions have showed almost more than 90% of the supplied materials were retained in the delta vicinity. On increasing the fine grain fractions, the deltaic deposits were decreased steadily, and it has lowered to about 70% when the fine grains have dominated 80% of the fraction. Figure 4-10 illustrates the relationships between the preservation potential and the longshore transported

sediments vs. the grain size fractions. The longshore transport reveals that the sediments have drifted alongshore from ~60 km to more than 130 km, when the fine grains have increased from 10% to 90%. The Isopach map of Figure 4-11 confirmed the grain size effect on the subaqueous morphology. At 90% coarse grains (top picture), most of the sediments were piled up around the river mouth, while at 10% of the coarse grains (lower picture), the stratigraphy was well distributed along the shelf and an elongated subaqueous delta was developed. Thought the analysis reveals big morphologic change, the shelf deposits have a narrow volume change as response to grain size effect (ca. range of 25%). This indicates that the model was more effective on transporting the fine sediments longshore over the shelf, where most of the deposits were preserved.

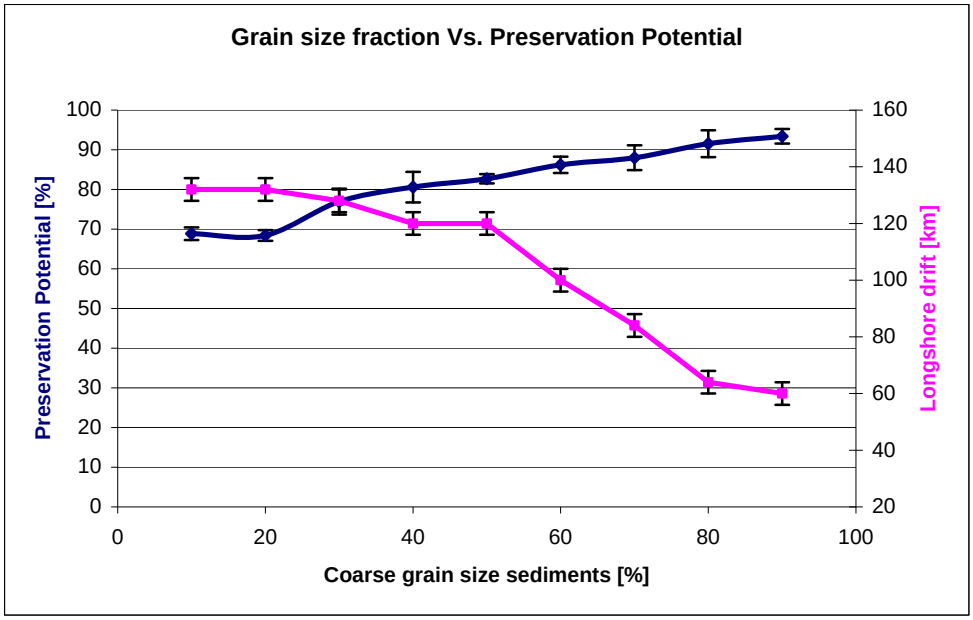

Figure 4-10: Grain size effect on preserved shelf sediments with their STDEV.

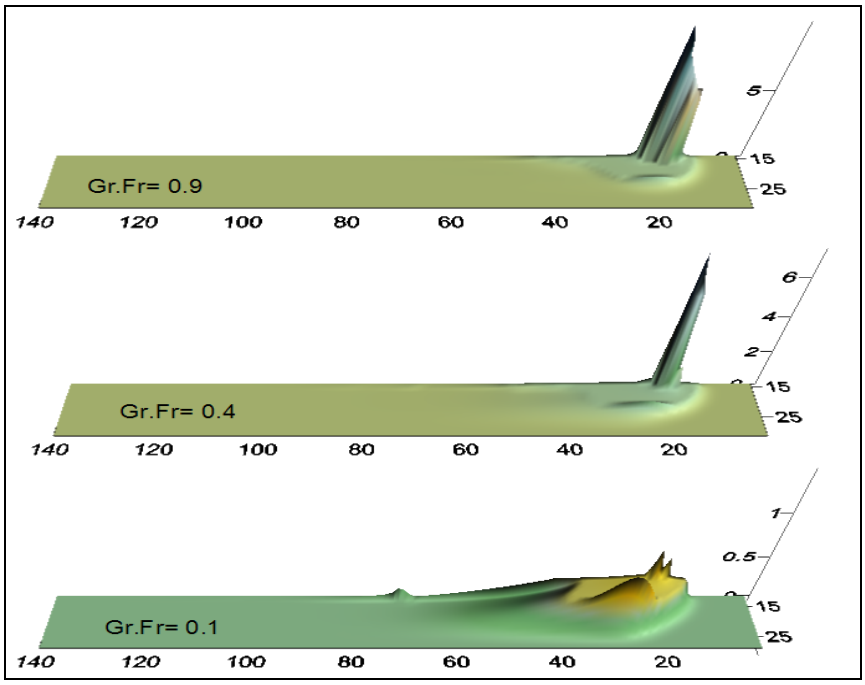

Figure 4-11: Isopach map of grain size assessment on marine domain (N.B. different vertical scales)

4.6 Experiment-6: Comprehensive-Multiple River Analysis

Since the focus of the research is to simulate the sedimentary architecture of the Adriatic basin; the setup of this scenario has combined all of the optimal parameters of the above experiments that could reproduce a longshore prograding subaqueous depositional architecture, similar to the Adriatic deposits. From the simulation of the five experiments, the factors that have preserved more than 60% of the reworked sediments on the wave stabilized proximal shallow-shelf have been chosen to simulate a comprehensive multi-river model. The input parameters are displayed in Table 4-1 as experiment-6, and these factors are comparable to the Adriatic basin parameters. The shelf gradient and width of the model resembles the northern Adriatic shelf, while the hydrodynamic factors and fluvial property are also consistent with the conditions of the Adriatic system. A basin scale morphology and stratigraphy development of the scenario has been interpreted and the isopach map of the scenario is shown in Figure 4-12. The avulsion features on the continental part were accurately simulated. As a result, a lobe-switching system of cyclically changes forcing in the marine domain (between of 15 and 25 grid-cell latitudes) with elongated plume deposits have been formed. The map also displays subaqueous morphologies that have prograded alongshore under the hydrodynamic forces on the marine domain. On the deep marine part of each delta (between 25 and 30 gridcell latitudes), patches of remnant sediments were illustrated. These deposits were dispersed to the deep shelf below the wave base.

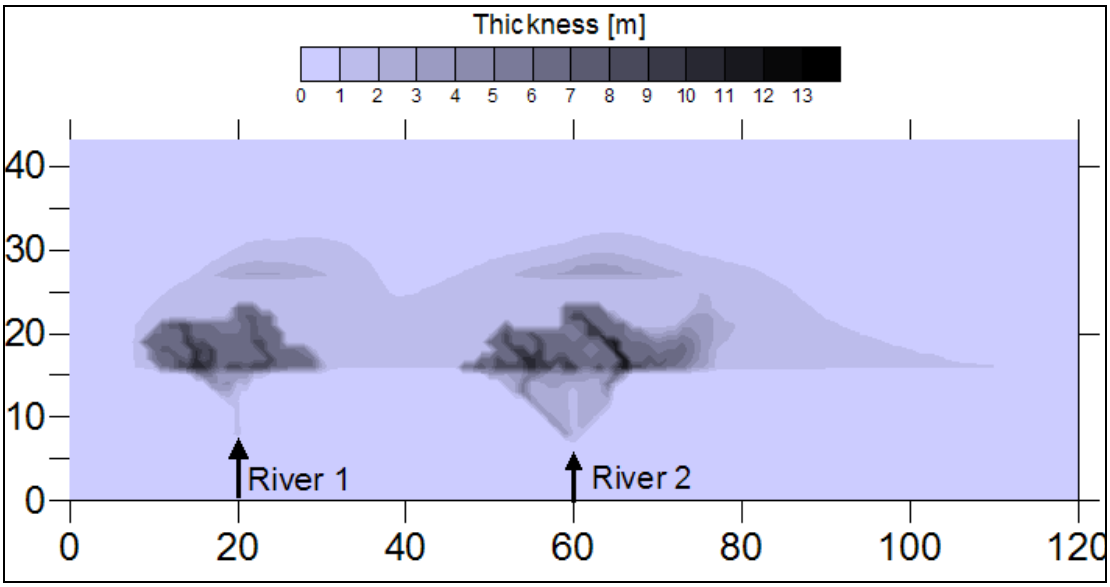

Figure 4-12: Isopach map of comprehensive multi-river system. [scale 1 gridcell=4 km].

The current map of the model has been interpreted to examine the fluvial flux effects on the general sea-current fields. Figure 4-13 reveals the rivers flux has small impact on the basin current field; where the flow potential has been decreased lineally throughout the basin. It was indicated by longer arrows in the entry point and was decreased all along the basin. At the outflow boundary, coastward deflected current fluxes have been illustrated. This phenomenon was consistent with the isopach map where very small deposits have been piled up at the end margin of the basin. This effect should be regarded as a boundary artefact / wall effect, since it was a closed system.

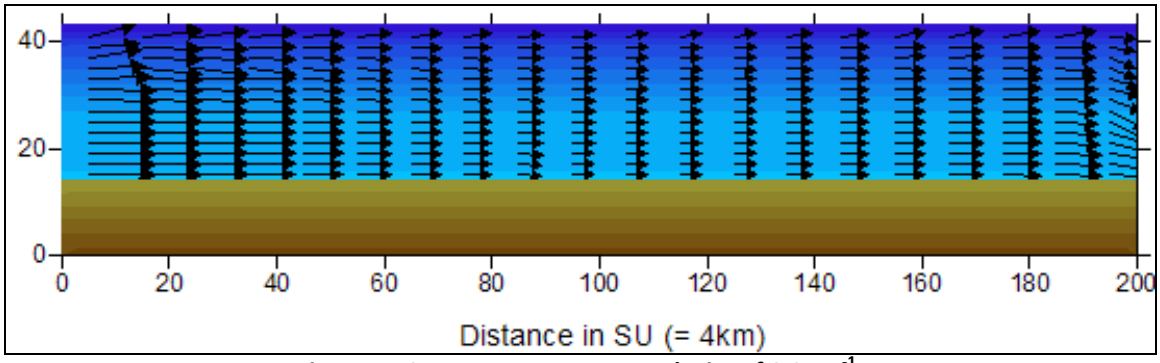

Figure 4-13: sea current map at velocity of 0.3 ms^{-1}.

To understand an impact of any current barrier structure on the substratum (such as promontory or headland or prograding delta), the discharge and sediment load of the first river supply was increased. The result showed almost identical current flux, except it created a larger delta. Again a reversal test was done in which the first river was reduced by half. The stratigraphy of both deltas developed well without affecting the depositional morphology of each delta. This test indicated that the marine conditions were invariable in the entire routine of the model where the flow field remains stable

under the conditions of delta progradation. But the flow field near of the river plume entry has been affected by the fluvial discharge velocity, which eventually stabilized with the general current field farther offshore from the river apex.

4.7 Summary of the Analysis

The calibration experiments of the initial and boundary conditions of the model have shown a wide range of sensitivity and depositional responses. A summary of the experiments is given below.

- Longshore morphology was highly sensitive to the basin gradient, sea current velocity and grain size fraction, (respectively experiments 1, 4 and 5).

- Shallow gradient-shelves are strongly influenced by sediment reworking, and has produced a wide and relatively thick preserved morphology, (experiment 1).

- In wide shelves, the model can transport the fine materials offshore more than 76 km, (experiment 2).

- Wave action is more effective in transporting sediment offshore than longshore (experiment-3). During the experiments, deep sea wave height of less than 4.2m has similar impact in sediment dispersion to the deeper shelf where patches of deposits were preserved under the wave base. This effect is due to the wave base parameterization of the model which has a base depth of around 6m in the specific synthetic basin geometry.

- On shallow marine basins subjected to a high current velocity, (experiment-4), patchy coastal deposit has been shown. This could be generated possibly when the avulsion in fluvial system was directed in the downstream direction of the current field. The process was highly pronounced in experiment-6 where the model had simulated lobes of elongated plume deposits developed in the proximal shelf.

- The flow field of the sea-current was stable in the entire routine, and the flow potential decreases linearly at a constant gradient along the entire basin.

- Sediments dispersed to the deeper part of the shelf were preserved throughout the routine and had a similar morphology in all of the experimental scenarios. These sediments were deposited below the effective wave/current base and were unaffected by the hydrodynamic properties of the model.

Overall speaking, the calibration of the model on the synthetic basin has provided an insightful understanding of the boundary conditions. Single values should not be used for the simulation purpose as the parameters are not independent. Different combinations of the calibrating parameters may give nearly identical results. For a real sedimentary basin simulation, the parameters should be from a basin data records that

persisted in equilibrium for its entire geologic history. This may also reduces the uncertainties during the simulation.

The Adriatic basin has been in equilibrium since the Late Quaternary, and the basin wide continental and marine characteristics of the Adriatic have all of the controlling parameters of the model to simulate its stratigraphy. The factors in scenario-6 were mainly adopted from Adriatic data; and the results indicated that the model has a capacity to reproduce a subaqueous stratigraphy, which was formed by similar depositional processes that occur in the western Adriatic shelf. For a complete Adriatic stratigraphy modelling, different combinations of the continental and the marine factors have been simulated. The next part of the project deals in detail with the simulation procedures of the different scenarios, and interpretations of the depositional results for the complete, basin-scale Late Quaternary Adriatic stratigraphy.

Chapter 5: Application to the Adriatic Basin

5.1 Calibration Approach

The chapter describes the calibration and application of the numerical model to the Adriatic Basin. Adjustments of the fluvial supplies, marine conditions and bathymetry profile for an efficient simulation, and the simulation procedures are discussed in detail.

5.1.1 Bathymetry and Substrate Sediments

The bathymetry of the Adriatic basin was arranged so as to simulate the mud wedge deposits on the western continental shelf. For an efficient computational time, the land parts far from the coast and the deeper part of southern basin are excluded. Since the numerical model was parameterized in 4*4km gridcell size basis, a bathymetry of 600 km long and 264 km wide with gridcells of 4*4km was extracted, Figure 5-1. The extent of this basin comprises position of the Late Quaternary deposits of the Adriatic basin. Different simulation scenarios has been treated (Table 5-2) and the grain size distribution of the seafloor substrate sediments had covered 20% to 80% of clay to medium silt (fine sediments) with a thickness range of 0.5m to 2m. These characteristics of the bathymetry encompass the preserved northern and central-western Adriatic shelf deposits. The relative sealevel curve of (Figure 5-2) derived by Storms et al. (2008) was adopted during the simulation. The curve shows different rates of sealevel rise or transgression rates on the shelf. These features coupled with the nature of the bathymetry profile were important to define the current flow boundaries.

5.1.2 Sediment Sources and Supplies

The model uses two classes of grain sizes, and the clay to medium silt size sediments of Adriatic were considered as one ‘fine particles’ class, where as the coarse-silt to sandy parts as a ‘coarse’ fraction. In the simulation, all of the fluvial sediments were considered to comprise ~80% of fine and 20% of coarse materials. These are consistent with the literature data of (Brommer 2009 and Milligan et al. 2007). The numbers of rivers that drain to the Adriatic shelf are so numerous that simulating all is time inefficient. In the project, the river positions were modified and priority was given to the 10 main and effective rivers that have relatively higher fluid discharges. The Po River and other relatively major rivers were set to be at their original positions and the sediment supply rates of the nearby small rivers were added to them. Rivers on the northern shelf are added to the Tagliamento River. The Adige and the Po Rivers are added together at the Po River. Fluvial supplies south of the Po and on central-western shelf were summed to seven main rives and one for area south of the Gargano Promontory, Figure 5-1. This adjusted allocation of the rivers results in a uniformly distributed sources of sediments along the western shelf.

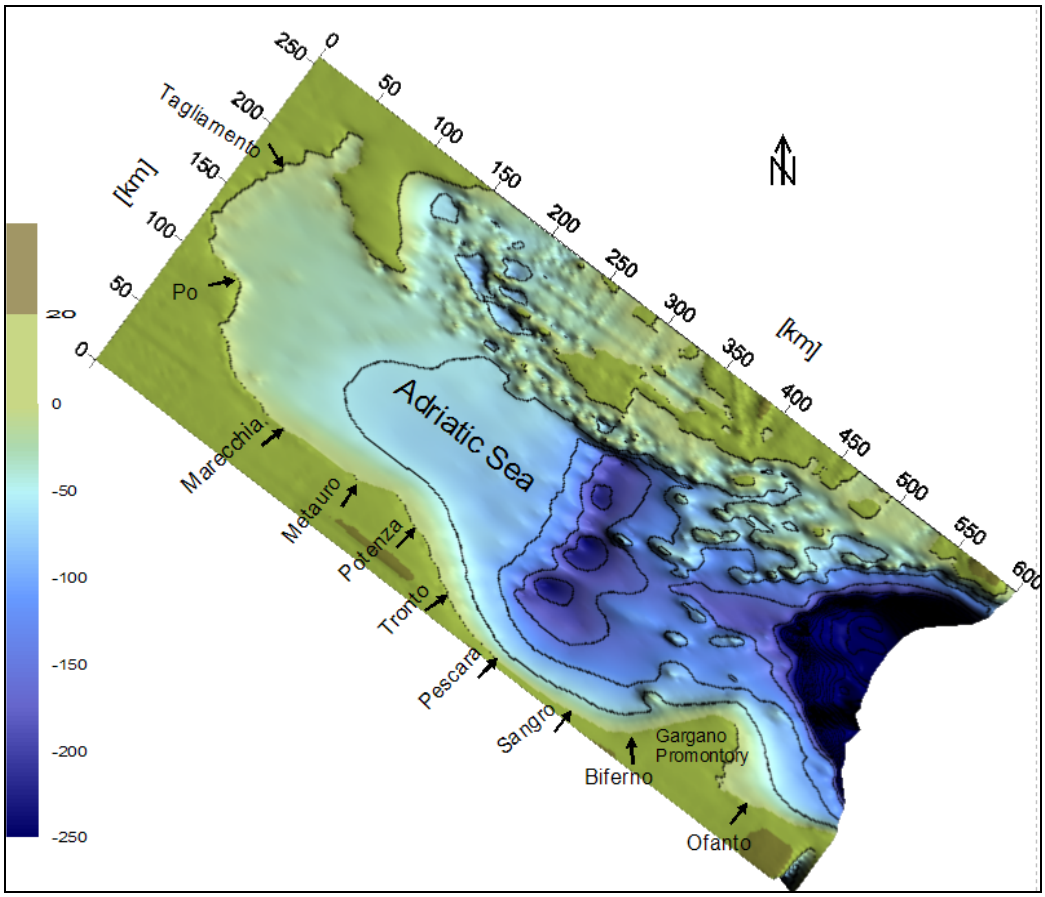

Figure 5-1: Extracted Adriatic basin bathymetry and positions of 10 main rivers on the western shelf.

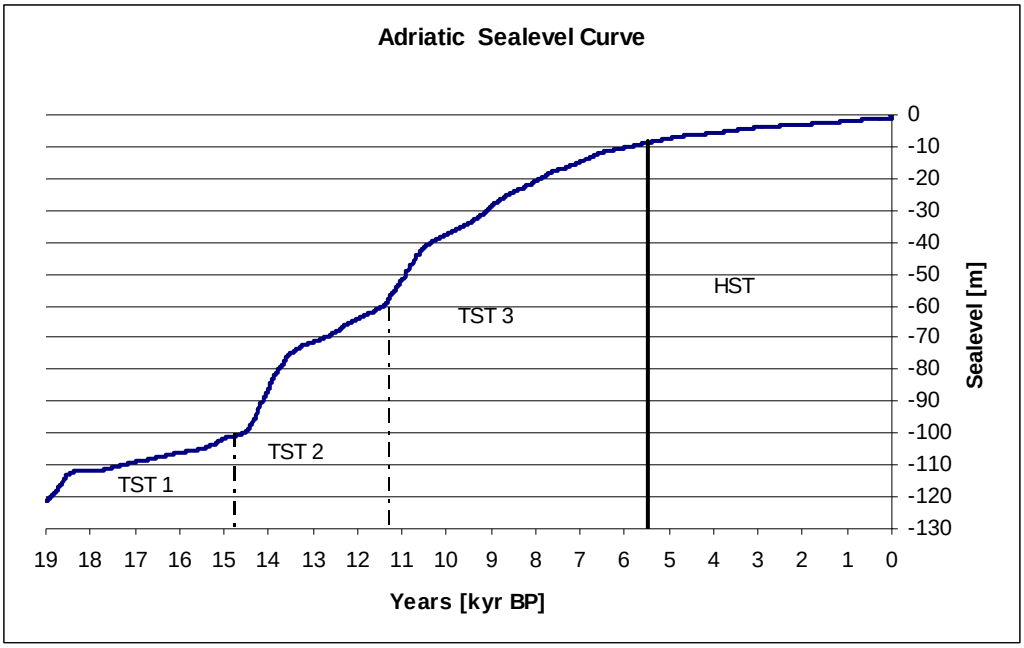

Figure 5-2: Relative sealevel curve of Adriatic Sea (Storms et al. 2008) and four temporal Systems Tracts (Brommer et al. 2009).

During the simulation, the amounts of sediment supplied by the rivers were extracted from the literature and average supply rates were used. For the recent times of 5.5 kyr BP to the present, sediment characteristics from the report of Brommer et al. (2009) were used as a main source reference in addition with reports of Syvitski et al. (2007) and Harris et al. (2008). During the earliest periods of 19 kyr BP to 5.5 kyr BP, the supply rates were estimated from basin wide sediment mass balance reports of Brommer et al. (2009) and partly form Cattaneo et al. (2003). The supply rates were subdivided into five units in order to be consistent with the deposits and follow the development of the Adriatic stratigraphy according to the subdivision of the lithosomes, (Brommer et al. 2009 and Correggiari et al. 2001). A summary of the applied supply rates and total fluvial loads for each of the simulations is given in Table 5-1. The liquid discharges were adopted from the recent century records, and the values have been adjusted proportional to the river loads which were adequate to carry the sediments to the marine environment.

Table 5-1: Liquid and sediment supply rates to the Adriatic basin from the 10 selected rivers.

Rivers		Tagliamento	Po	Marecchia	Metauro	Potenza	Tronro	Pescara	Sangro	Biferno	Ofanto	Total
Liquid discharge [m3/s]		40	160	30	30	30	30	30	30	30	10	
19 to 14.8 kyr BP	Rate [Mt/yr]	1.1	17.7	2.2	2.4	2.4	1.9	1.9	1.9	1.9	0.6	33.9
	Total [Gt]	4.6	74.3	9.2	10.1	10.1	8.0	8.0	8.0	8.0	2.3	**142.5**
14.8 to 11.3 kyr BP	Rate [Mt/yr]	1.2	19.7	2.8	2.9	2.9	2.4	2.4	2.4	2.4	0.8	39.9
	Total [Gt]	4.3	68.8	9.8	10.2	10.2	8.4	8.4	8.4	8.4	2.8	**139.6**
11.3 to 5.5 kyr BP	Rate [Mt/yr]	1.2	19.6	2.4	2.8	2.8	2.1	2.1	2.1	2.1	0.6	37.9
	Total [Gt]	7.1	113.5	14.2	16.0	16.0	12.4	12.4	12.4	12.4	3.5	**220.0**
5.5 to 0.4 kyr BP	Rate [Mt/yr]	1.7	27.8	3.5	3.9	3.9	3.0	3.0	3.0	3.0	0.9	53.8
	Total [Gt]	8.8	141.5	17.7	19.9	19.9	15.5	15.5	15.5	15.5	4.4	**274.2**
0.4 kyr BP to Present	Rate [Mt/yr]	1.7	17.3	3.0	3.5	3.5	3.0	3.0	3.0	3.0	0.9	42.1
	Total [Gt]	0.9	8.7	1.5	1.7	1.7	1.5	1.5	1.5	1.5	0.4	**21.0**

5.1.3 Marine conditions and Hydrodynamics

In literature hydrodynamic conditions of the Adriatic basin just for the recent centuries were reported. Storms et al. (2008) have indicated a linear relationship of the paleo-wave ratio of the Adriatic basin to the present day values. The wave height ratio rose simultaneously with the position of the retrograding shoreline. This relationship of wave and transgression over the shallow northern shelf has illustrated the development of the hydrodynamic conditions to the present day full capacity. In the simulation, present day current conditions of the basin are then used in a similar manner to estimate the paleo-current conditions which represented the development of the prevalent current of Adriatic basin (WACC).

The WACC is the main sediment conveyer in the basin. It experiences a favourable and anti-gyres wind effects respectively during winter and summer. Since the model uses an annual storm-based hydrodynamic algorithm, the Bora wind (winter storm) intensified a continuous southward flowing current along the Italian coast is implemented. A user defined no-flow boundary was adopted at the centre of the Adriatic basin. It separated the incoming current along the east coast and the outgoing flux towards the Gargano Promontory along the western coast, Figure 5-3. The end of the current boundary and the current flux values for each time steps were assigned depending on the relative sealevel curve and the paleo shoreline positions. Hence, the marine conditions have simulated the development of the WACC from its start to the present day conditions. For the time interval of 19 to 14 kyr BP the current velocity value was set to zero, since the WACC became active at around 14 kyr BP after the sealevel rise (Cattaneo et al. 2003). After 14 kyr BP, starting transgression of sea over the shallow northern shelf, both the length of the current boundary and flux values are increased linearly with respect to the paleo shoreline positions.

5.2 Simulation Scenarios

A wide range of factors have been calibrated to simulate the Adriatic stratigraphy. The scenarios are summarized in Table 5-2, where the first row of the table shows the range of the tuned parameters. The fluvial system was characterized between 70% and 90% of clay to fine silt sediments. The model had more or less similar stratigraphic effects on these ranges. Therefore, 80% of the fine fraction was chosen for the optimal simulations, which was also consistent with the actual Adriatic sediment characteristics. The model uses an annual deep-sea wave height algorithm; and in the calibration wave heights between 3.8m and 5.0m were treated. These values were from the wave height records of the Adriatic Sea and are consistent with the effective values of the synthetic model. In all the simulation, the current velocity has been affected highly by the liquid discharges of the fluvial system. To use the adjusted fluvial liquid discharges, the total magnitude of the sea-current velocity needed to be higher from the present-day conditions of the Adriatic Sea, which is ~ 0.2 ms^{-1}. Lower velocities have created a reversal of flow potential, especially the northern Alpine and Apennine rivers discharged their flux to the

southern part of the basin and greatly influenced the basin-scale circulation pattern. Therefore, it was necessary to have on-hand a fluvio-marine balanced flux potential of a basin for an application of a full-scale circulating system before applying the model. During the experiment, the adequately balanced basin scale current velocity has been adjusted to more than double of the present day velocity. The boundary line of the circulating current has been also adjusted through its development course to allow sufficient circulating flux; which was crucial for the longshore sediment transportation, Figure 5-3.

Table 5-2: Calibration scenarios for Adriatic stratigraphy modelling

Scenarios	Fine grain fraction of the fluvial system	Deep sea wave height [m]	Current flux velocity [ms^{-1}]	Substratum characteristics	
				Thickness [m]	Coarse fraction
Assessed ranges	**70-90%**	**3.8 - 5.0**	**0.1 - 0.6**	**0.5 - 2**	**10 - 30%**
scenario-1	80%	4.5	0.6	2	20%
scenario-2	80%	4.5	0.3	2	20%
scenario-3	70%	4.2	0.6	0.5	30%

Most of the combined-parameters simulations have similar effect on the morphology, and many of the scenarios results were unrealistic when compared to the actual stratigraphic architecture of the Adriatic. Higher hydrodynamic values have greatly eroded all of the coastal zones and sediments were deposited at the centre of the basin as deep as ~40m isobath. Lower values also made the model unstable for further iteration. After each simulation, the results of the model had been interpreted; and the factors of the scenario were then adjusted to re-run a modified scenario. This calibration procedure was repeated until the model produced the geomorphological result similar to the Adriatic units. From the various simulations, three optimal scenarios of realistic results are chosen for discussion.

In all of the three scenarios, the basic pattern of the WACC (the oceanic-current) was simulated and was characterized to flow south-eastward along the western shelf, Figure 5-3. The map displays present day current conditions, which is fully developed basin-scale hydrodynamic capable to rework and transport the sediments along the shelf. After this hydrodynamic condition was adjusted efficiently, the model was then set to simulate the complete Late Quaternary sediments of the basin.

Surfer graphic software was used to visualise and interpret the results of the simulated scenarios, and *Excel worksheet* to quantify the sediment mass and their uncertainties along the Western Adriatic shelf. During the interpretation and volume estimation of the results, great concern was given to minimize any systematic error that could originate from statistical procedures. *Kriging* method with *Spherical Variogram Model* was the best candidate for grid model that was served as a fundamental internal data representation (Golden software, 2002). An example of the Spherical Variogram model with experimental data of the isopach and spatial grain-size distribution maps are shown in Figure 5-4.

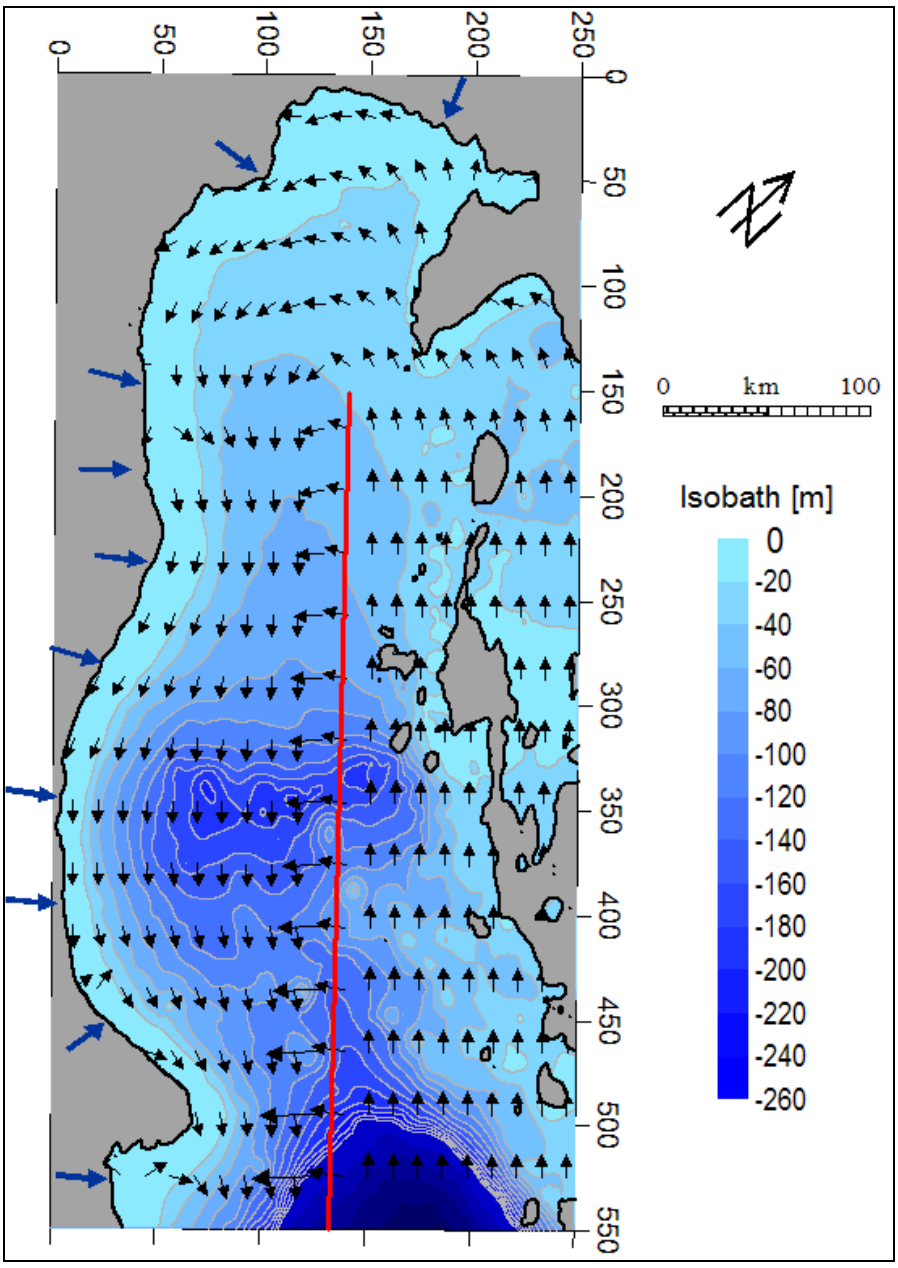

Figure 5-3: Present day longshore counter-clockwise circulating current field with river positions; red line indicates position of the no-current flowing boundary.

The model results were in gridcell size of 4*4 km basis that has produced irregular (bumpy) surface maps and high uncertainties in sediment volumetric calculation. The spherical variogram model with a grid-cell size of 0.5*0.5 km has been used to interpolate the results. This denser grid technique has produced relatively smoother and continuous maps, which also reduced the uncertainty in volume calculation, (Golden software, 2002). The procedure was repeated during the interpretation of every

stratigraphy maps, grain-size distribution maps and current flux maps of all the scenarios.

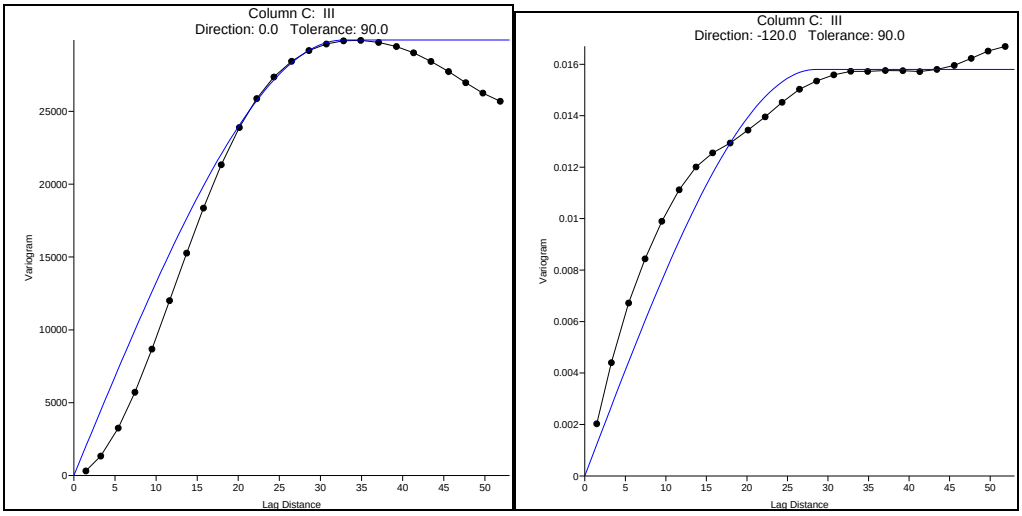

Figure 5-4: Spherical (blue) variogram model fitting the experimental variogram (doted) during interpolation of the isopach and the grain-size distribution maps respectively.

The maximum flooding surface at about 5500 years BP, separating the stratigraphy of HST from TST, was used as a temporal boundary to simulate the Late Holocene deposits for 5500 years. These sediments of 5.5 kyrs BP to the present (described as HST) are the most known and characterized shallow marine sedimentary units. Thus the model was calibrated to the conditions of the recent deposits; and it has reproduced the mud belt along the shallow western shelf. After simulating the recent time deposits, the model was then set to the conditions of 19 kyrs BP to 5.5 Kyrs BP deposits (described as TST).

The stratigraphic and spatial grain-size distribution maps and the sedimentation rate calculations for the last 5.5 kyr (HST deposits) of the three optimal scenarios were interpreted. Figure 5-5 displays the Isopach maps of the three scenarios, which were simulated for 5500 years. During the simulation, data of Table 5-1 and sealevel curve of the Late Holocene and hydrodynamic values of the present day conditions were adopted. The maps display longshore elongated sedimentary units on the northern shelf and fan-shaped plume deposits around the central Apennine part of the western shelf. Scenario-1 shows deposition relatively close to the shoreline along the entire basin. Moreover, it shows preserved deposits south of the Gargano Promontory which is not present in the latter two scenarios. Scenario-2 demonstrated that the stratigraphy has moved (shifted) offshore below the 20m isobath along the entire basin. Possibly due to the reduced current velocity which might increase the relative effects of cross-shore transporting algorithm of the wave. The extent of the deposit in scenario-3, especially on the northern shelf, was thinner than the two scenarios. This reduction of depositional width is a combined effect of the reduced fine grain sizes of the fluvial loads and the reduced thickness of the substrate surface material. This reduction of

seafloor material could indicate the contribution of the eastern coast seabed sediments that were transported with the water-current.

The spatial grain size distribution was also assessed to reveal the differences among the scenarios. Figure 5-6 displays the spatial coarse grain size distributions of the three scenarios after 5500 simulation years, (end of HST). The maps show big variations compared with stratigraphic results. Thought the results of scenario-1 and scenario-2 are comparable, the distribution of the coarse materials around the Po delta in scenario-1 is more elongated southward along the shore. The result of scenario-3 is completely different, where the coarser materials have been deposited close to the coastline of the entire basin. After the HST results were quantified, the model was set to the conditions of 19 to 5.5 kyrs BP, and has been simulated for 13,500 years to reproduce the TST deposits. The results of the three scenarios were also more or less similar to each other.

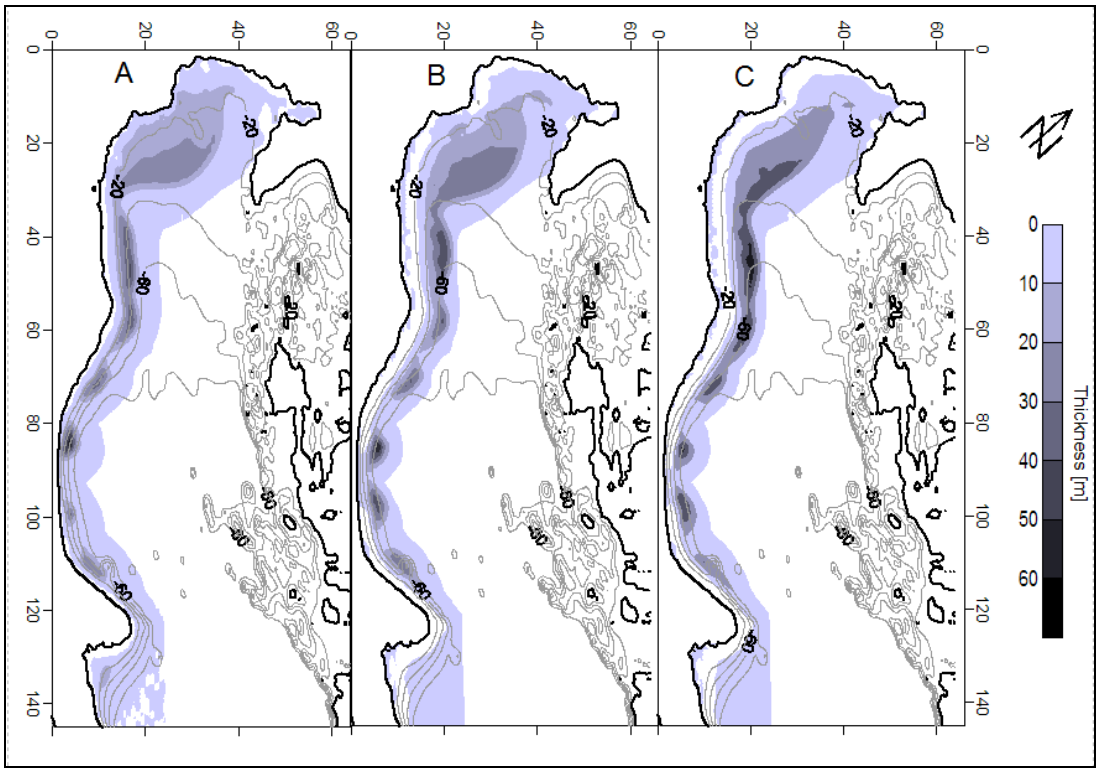

Figure 5-5: Isopach maps at the end of 5500 time steps: A) scenario-1, B) scenario-2 and C) scenario-3. [Scale 1 gridcell=4km].

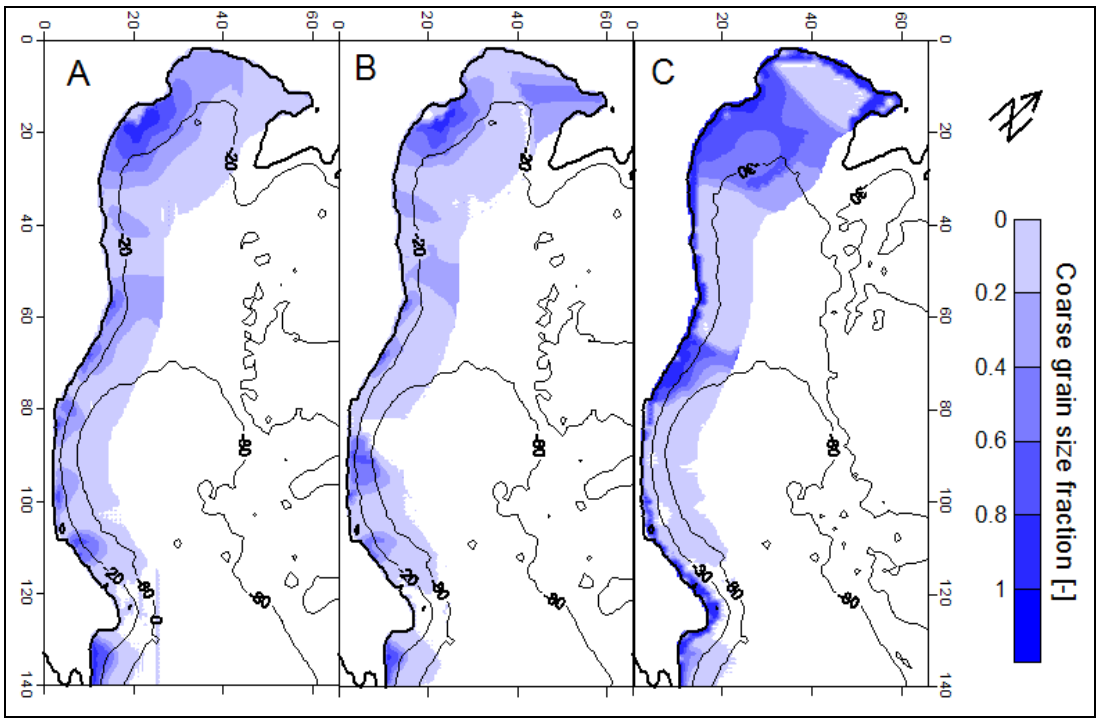

Figure 5-6: Spatial grain-size distributions at the end of 5500 time steps; A) scenario-1, B) scenario-2 and C) scenario-3. [Scale 1 gridcell=4km].

The stratigraphic results of scenario-1 have showed preserved sediments relatively closer to the entire shoreline. These deposits are similar to the mud belt on the Adriatic deposits and the spatial grain-size distribution is also more realistic result. Moreover, the estimated mass-balance was comparable with the literature data, and has shown a flux difference of only ±3.0 Mt/yr among the scenarios. Hence, scenario-1 is considered to be the most optimal scenario which can represent the stratigraphic architecture of the Adriatic basin. It has demonstrated the development of the Adriatic stratigraphic history and sediment transportation along the western Adriatic continental shelf. The results are discussed in detail in the next chapter.

Chapter 6: Results

In this section, results of scenario-1 are discussed in detail. The results demonstrate the morphological and stratigraphical development of the basin and spatial grain-size distributions in different time steps. Lithosomes of HST and TST units with their quantified depositional volumes are discussed separately in detail.

6.1 Geomorphology and Stratigraphy of HST

An isopach map of 5.5 kyr BP to present time (HST stratigraphic unit) is displayed in Figure 6-1. The sediments on the north-western shelf were deposited between 0 and 40m isobaths. On the central and south-western part of the shelf, sediments were preserved all between 20m and 80m isobaths. The deposition has a maximum thickness of ~45m around the Ancona-headland area. Sediments from the northern rivers (the Tagliamento and the Po rivers) experience both longshore and cross-shore transportation and have created a wider subaqueous delta. While the sediments around the central shelf (rivers of Marecchia, Metauro and Potenza) were more affected by the longshore currents and a delta prograding longshore was formed. Sediments from the central area (rivers of Tronto, Pescara, Sangro and Biferno), which were around the central Apennine part of the shelf, have lobes of fluvial-fan feature.

Two HST lithosomes were interpreted separately and the results are displayed in Figure 6-2. The isopach map of HST-1 (5.6 to 0.4 kyr BP) has similar morphology with the result of the complete HST. It is rational to expect such result, since the HST-1 comprises about 93% of temporal and sediment supply of the complete HST. Result of the HST-2 (0.4 kyr to present) illustrates that the deposit was less than 2m thick around the proximal deltaic area. Relatively thick deposits of 3m to 6m have deposited at about 40m isobath of the northern shelf. This could signify that the sediments were bypassing the delta-front area and moved to the prodelta part. The map also reveals that the progradation of the subaqueous delta was along the foresets which has developed southward parallel to the coastline.

6.2 Geomorphology and Stratigraphy of TST

The isopach map of 19 to 5.5 Kyr BP reveals two depositional centres for the TST deposits, Figure 6-3. The main depo-centre was the Mid Adriatic Deep (MAD) where the sediment thickness reached more than 90 m at its central part. The second depo-centre was located at the north-western wide shelf, which is relatively more exposed to the WACC. This unit shows longshore drifted deposits that have a thickness of about 30m. The MAD deposits show a thinning sequence to the westward parallel to the paleo-shorelines. This pattern could indicate the start of the WACC which was minimally activated during the early stage of transgression of the sea.

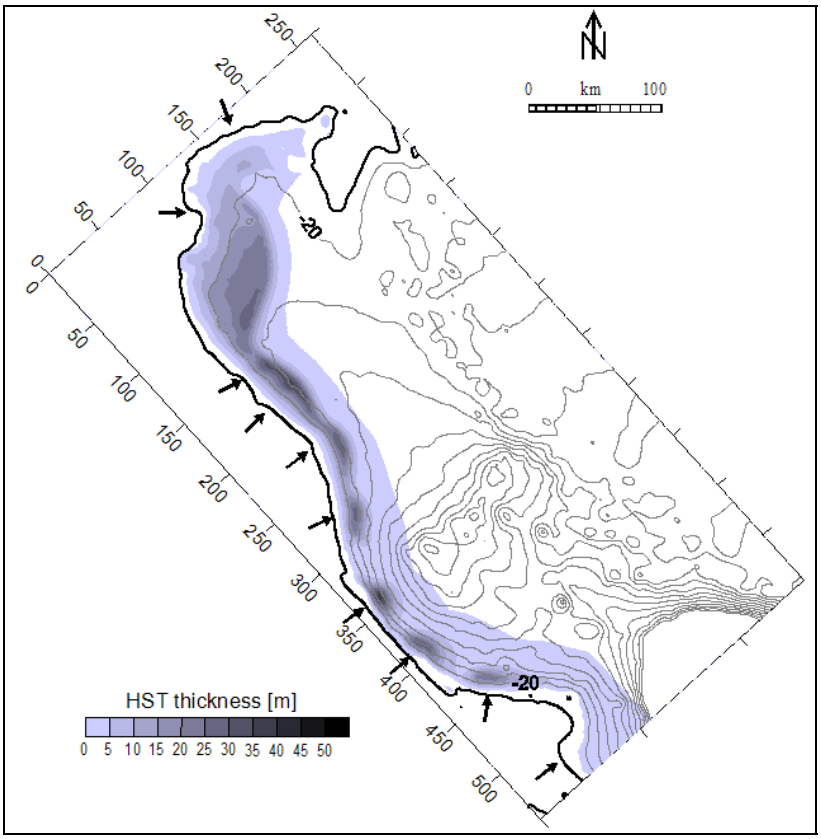

Figure 6-1: Isopach map of HST (end of 5500 yrs) with the river positions. [Contour interval 20m].

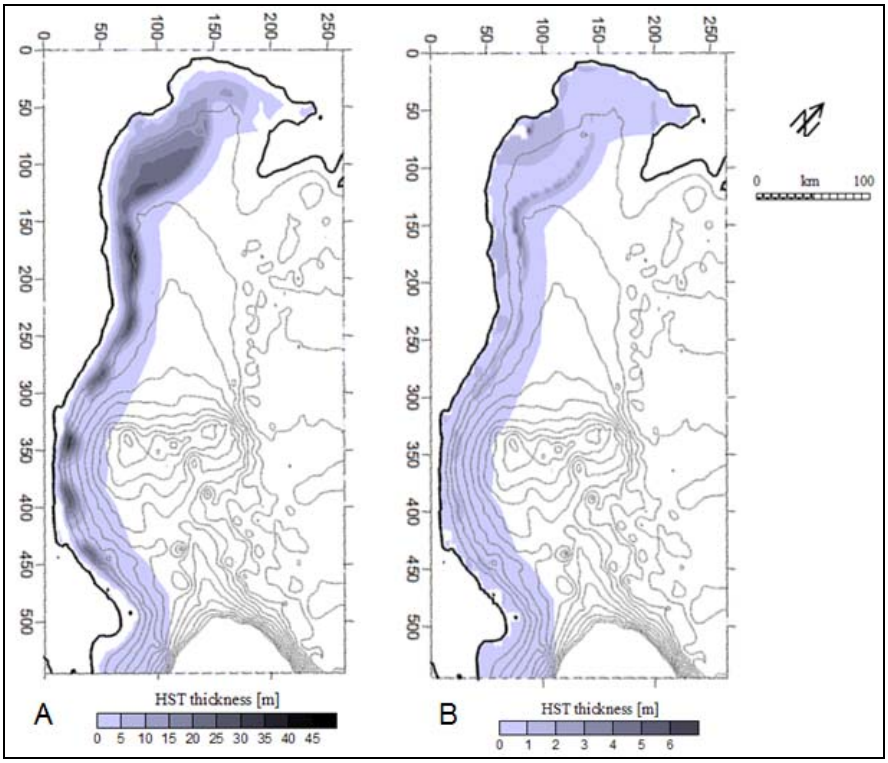

Figure 6-2: Isopach maps A) HST-1 (5.5 to 0.4 kyr BP) and B) HST-2 (0.4 kyr BP to present) indicates bottomset prograding subaqueous delta on the northern shelf.

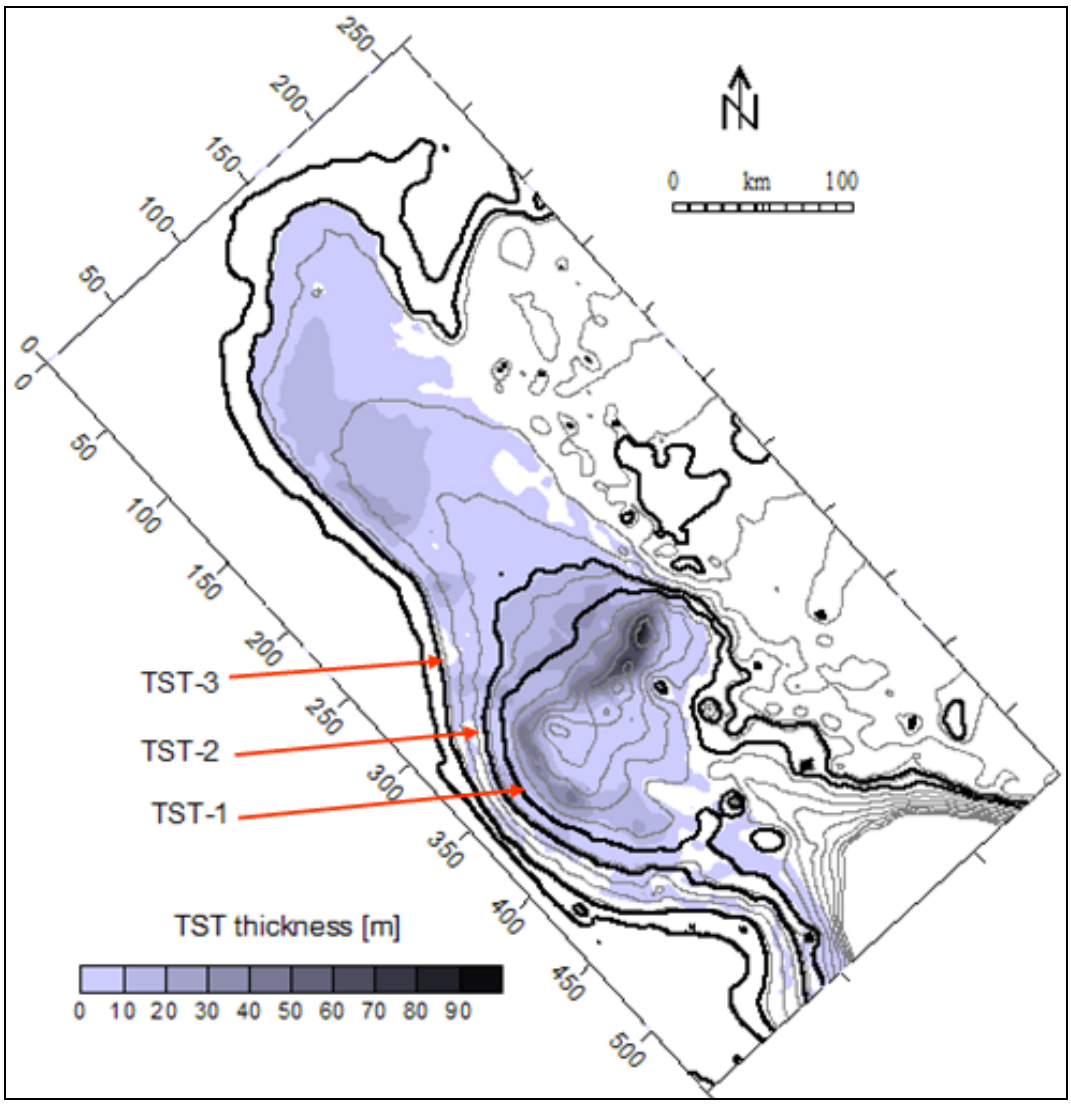

Figure 6-3: Isopach map of TST (after 13,500 years) with paleo-shoreline positions at the end time of each lithosome.

To illustrate the development of the TST deposits, three lithosome were interpreted separately. The 19 to 14.8 kyr BP deposits (TST-1 unit) were developed on the centre of the MAD and reach more than 70m thickness. At the end of the TST-1 unit, a minimal velocity of WACC was introduced and the system started to drift the sediments to the western paleo-shelf where the deposits reached a thickness of 40m, Figure 6-4. The 14.8 to 11.3 kyr BP deposits (TST-2 lithosome) were developed on the central shelf to a thickness of about 35m. On this shallow shelf, a north-westward thinning sedimentary sequence was developed. The central Apennine parts of the western shelf were characterized by fluvial-fan systems and reached a thickness of 25 to 30m. The 11.3 to 5.5 kyr BP deposits (TST-3 lithosome) were highly developed on the north-western shallow shelf and attain a maximum thickness of 30m around the Ancona headland. The deposits have a similar morphology with the isopach map of the HST deposit. Both

stratigraphies are characterized by subaqueous depositional processes which were developed on the shallow and wide shelf during the Late Holocene high sealevel. The central Apennine deposits of the TST-3 unit were characterized by channel deposits similar features with the TST-2.

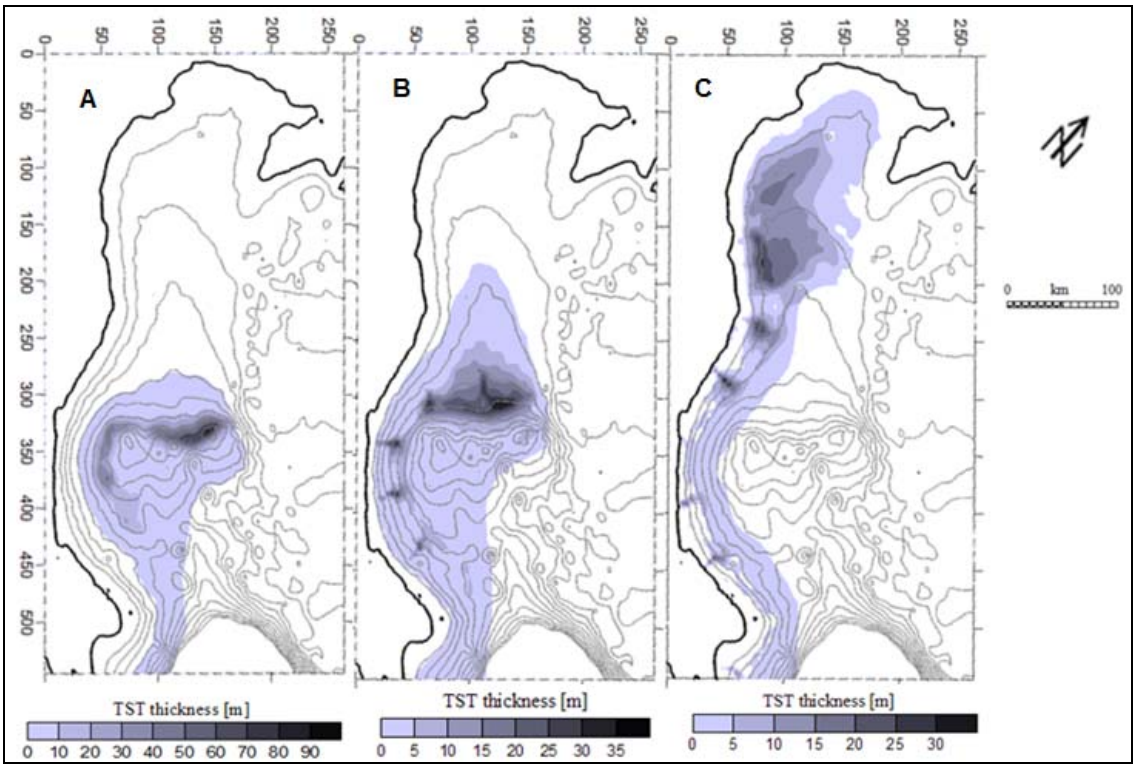

Figure 6-4: Isopach maps for the time span of A)19 to 14.8 kyr BP (TST-1 unit); B) 14.8 to 11.3 kyr BP (TST-2 unit); C) 11.3 to 5.5 kyr BP (TST-3 unit). [Contour interval of 20m].

6.3 Geomorphology and Stratigraphy of HST+TST

Continental and marine conditions of TST+HST were summed together to simulate the complete 19,000 years deposits. The results were interpreted to examine the complete Late Quaternary Adriatic stratigraphy development. Isopach maps of the four lithosomes are displayed consecutively in Figure 6-5. The map has revealed two depositional centres in the basin. The older deposits were preserved on the central and western part of the MAD, and starting 14 kyr BP, the depo-centre has moved to the shallow central and northern shelf. The MAD deposits are similar to the results of TST-1 and TST-2 as most of the sediments were deposited at the centre of the depression. The northern shelf sediments were shore hugging subaqueous deposits of roughly 40m thickness.

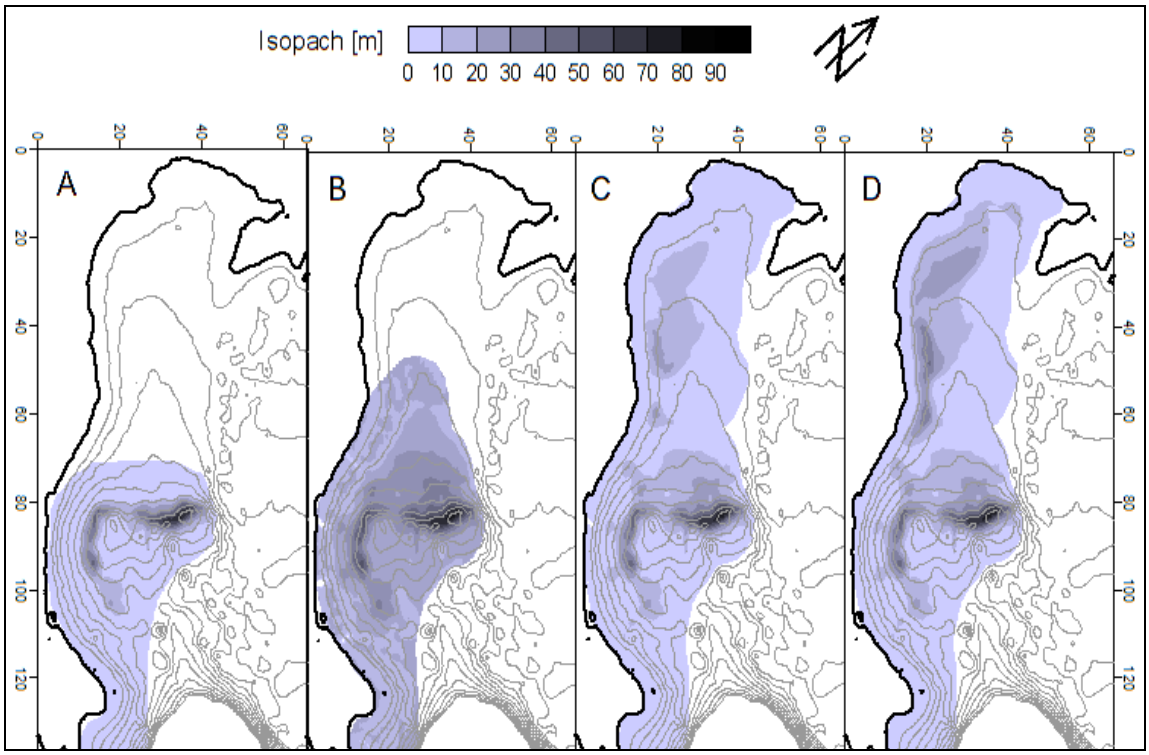

Figure 6-5: Isopach maps at the end time of A) 14.8 kyr BP, B)11.3 kyr BP, C) 5.5 kyr BP and D) present day. [Scale: 1 gridcell= 4 km; contour interval of 20m].

6.4 Spatial Grain Size Distribution

Spatial grain sizes distribution of the TST and HST units were examined and displayed separately in Figure 6-6 and Figure 6-7 respectively. The coarse sediments of the TST-1 unit were deposited primarily on the western part of the MAD and few coarse patches of sediments were preserved around the northern brim of the MAD. The maps of the TST-2 and TST-3 units display concentrated coarse patches of sediments on the northern shelf with few patches at the central Apennine part of the western shelf. The spatial grain size distribution maps for the HST sediments illustrated that most of the shelf area is represented by more than 50% of the coarse sediments. These coarse patches of sediment, especially of the central and southern shelf, correspond to the positions of the rivers and are almost consistent with the isopach maps. On the other hand, the northern shelf deposits have showed a fining trend to both cross-shore and longshore directions. It also proved the sandy materials have moved relatively to the south from their respective river positions.

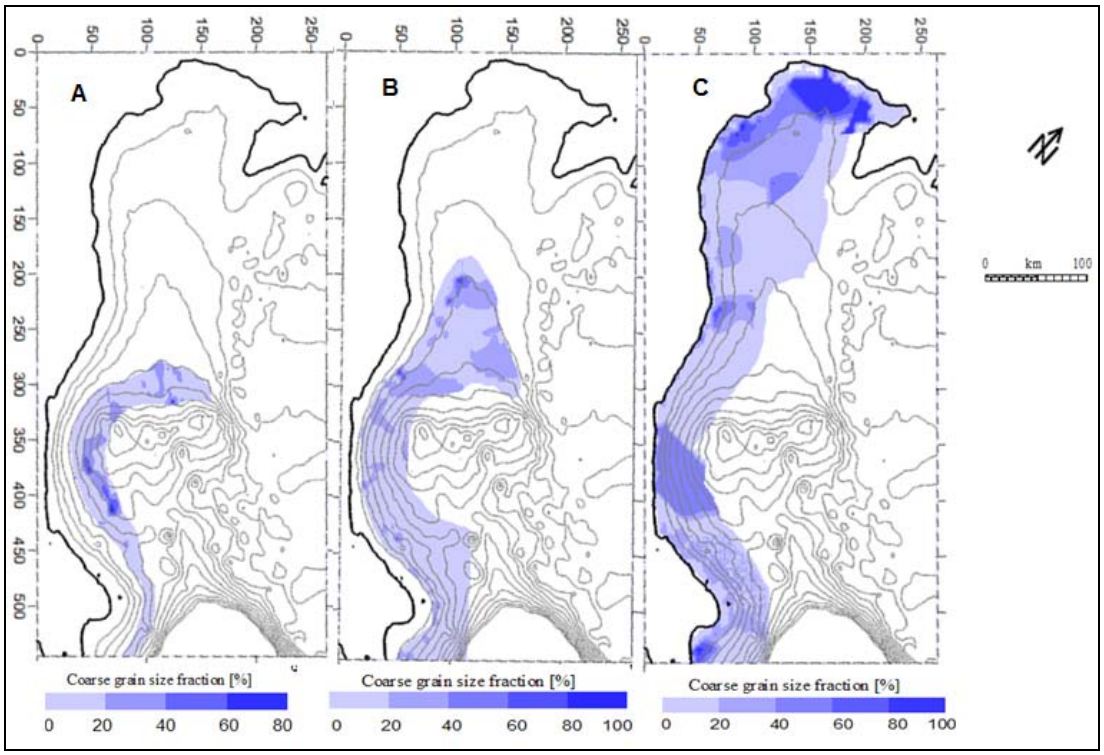

Figure 6-6: Spatial grain size distribution of the TST during the time step of: A) 14.8 kyr BP; B) 11.3 kyr BP; C) 5.5 kyr BP.

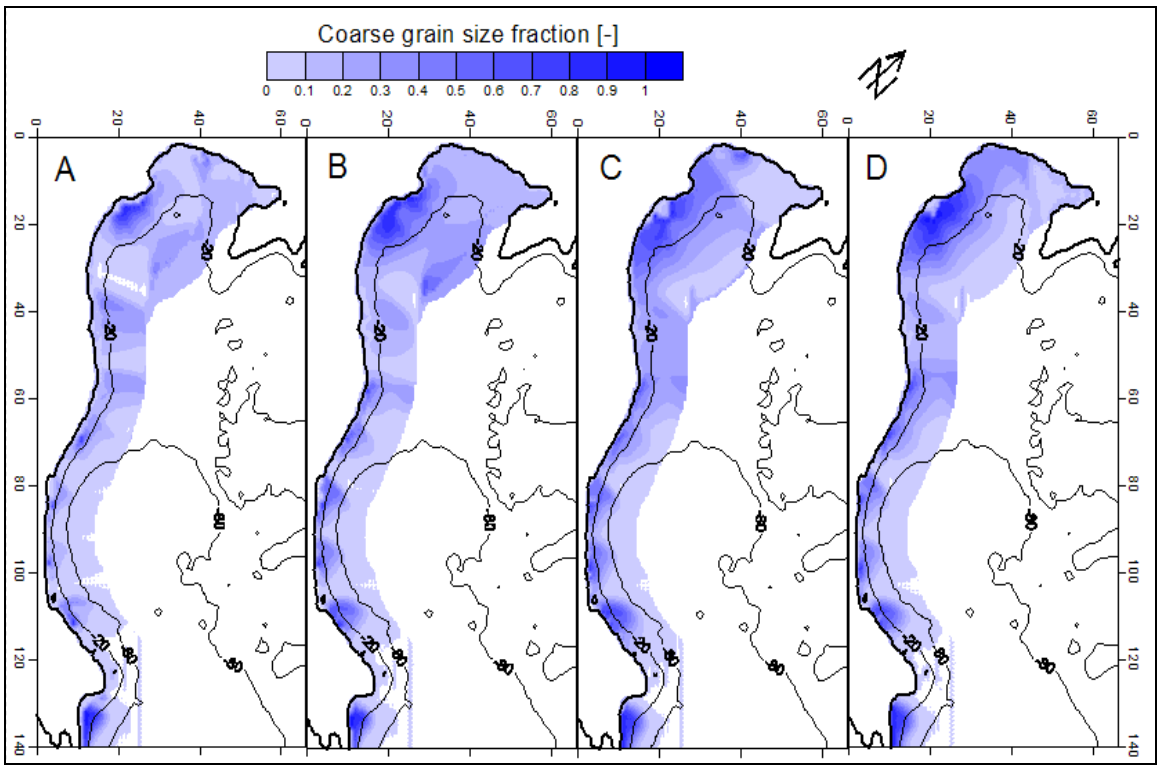

Figure 6-7: Spatial grain size distribution of the HST during the time step of : A) 4500 yrs BP, B) 3000 yrs BP, C) 1000 yrs BP and D) Present day. [Scale 1 gridcell=4km]

6.5 Stratigraphic Profiles along the Western Shelf

Three cross-sections have been chosen to investigate the Adriatic basin stratigraphic architecture. The profile lines are shown in Figure 6-8, where section A-A cuts the stratigraphy of northern shelf through the MAD parallel to the present day shoreline. Sections B-B and C-C cut respectively the subaqueous delta systems of the northern shelf and the deposits of central Apennine part of the western shelf. The profile of section A-A, Figure 6-9, shows that the TST system has noticeable thick patches of sedimentary units separated by a saddle structures. The saddle structures were generated by the wave-action, which was the prominent sediment reworking process in the model experiments. It has effectively eroded the shallow marine deposits and these saddle features possibly indicate paleo-shoreline positions. The HST deposits were preserved only on the stratum above the MAD (~260 km), and followed the surface of TST deposits. Section line B-B, Figure 6-10, cuts the subaqueous delta of the northern shelf. It reveals the delta has extended about 80 km offshore of the current coast. On the prodelta area, the HST units have a relatively steeper slope than the TST deposits. Around the coast, both units have erosional features on their respective substratum profile. These were also the wave action effects that erode and rework the seafloor surface sediments.

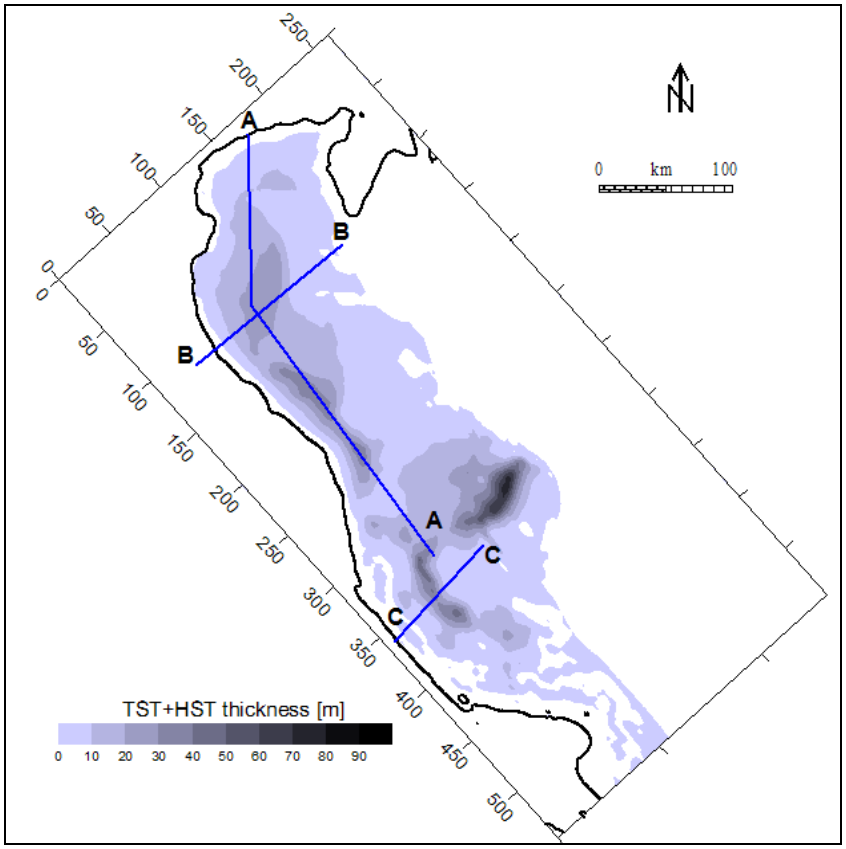

Figure 6-8: Cross sectional transverse lines along the Adriatic deposits

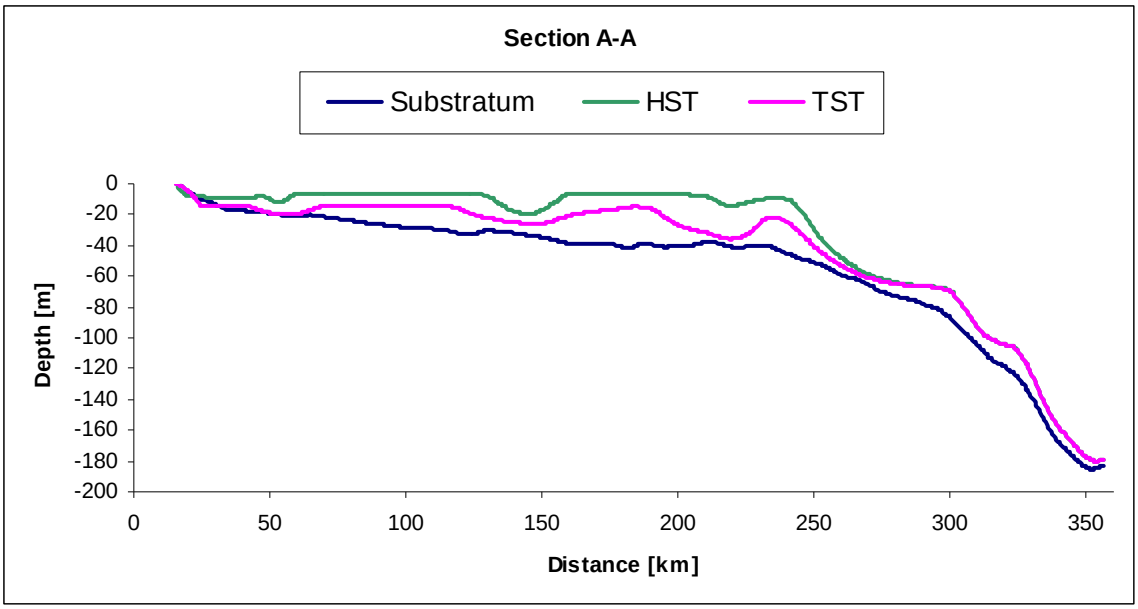

Figure 6-9: Profile of isopach map along section A-A

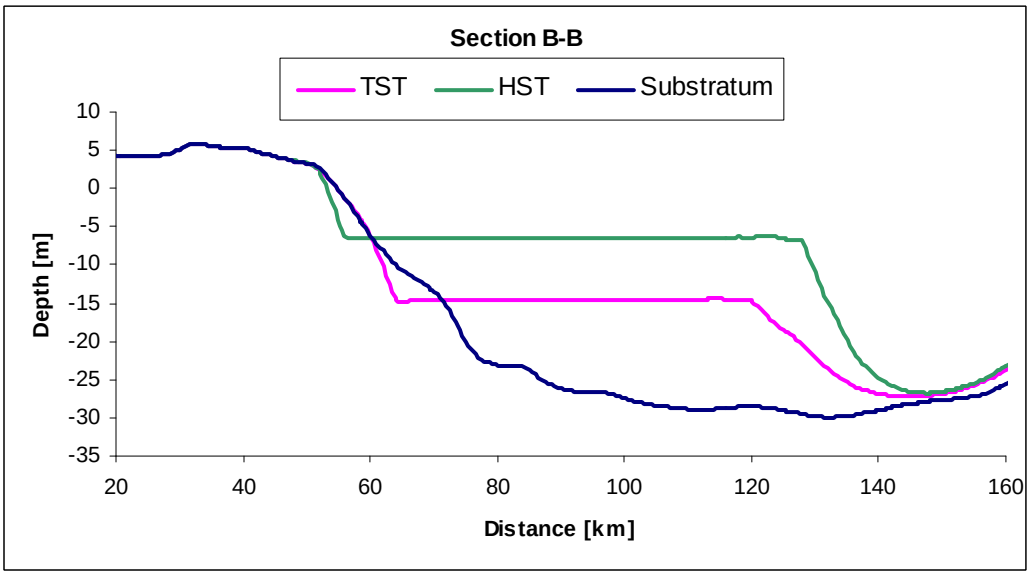

Figure 6-10: Profile of isopach map along section B-B

The wave action effect is also evident in the profile of section B-B and the HST profile in section A-A that has produced a flat topped stratigraphy. These deposits were formed during the Late Holocene when the sealevel has risen almost to the position of the modern shoreline. The water depth above the deposits became very shallow and coincided with the wave-base level of the model, which is ~ 6m. Hence, the materials above the wave-base level have been subjected to erosion and transportation for prolonged time and created a levelled topography. Section C-C of Figure 6-11 depict only the TST sediments, as these were preserved offshore of the central Apennine part of the western shelf, with a maximum thickness of about 45m along the western part of

the MAD. This deposit represented the TST-1 stratigraphy which was deposited at a lower sealevel. Upon transgression, (above 80m isobath) the substratum profile was also eroded.

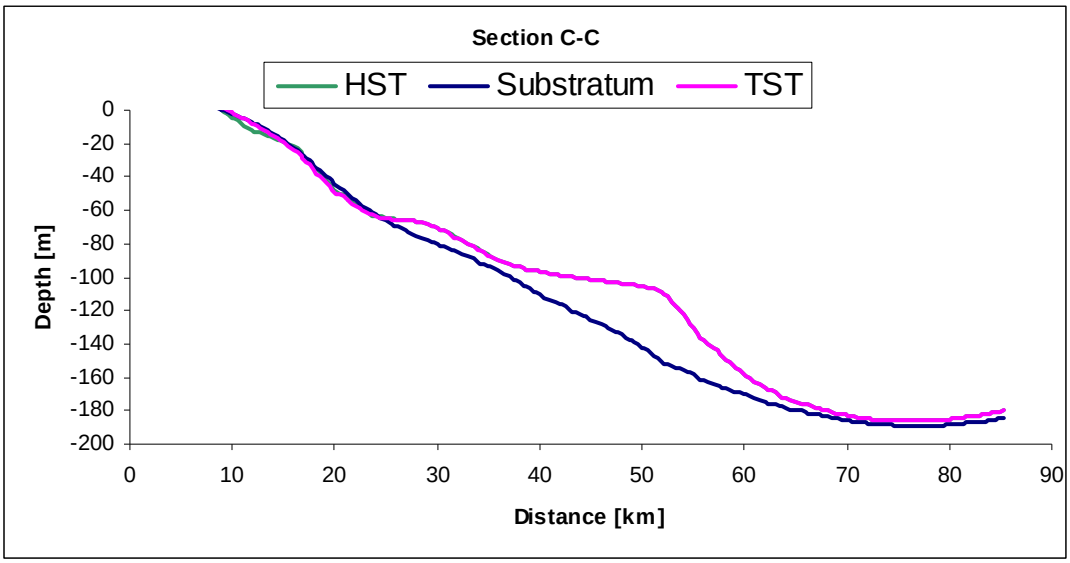

Figure 6-11: Profile of isopach map along section C-C.

6.6 Sediment Flux along the Western Shelf

To understand the combined wave and current actions in transporting the sediments along the western Adriatic shelf, sediment flux assessment has been done on the results of the HST unit. The shelf area was subdivided into five boxes that allow good spatial distribution of the fluvial entries. The offshore extent of the boxes was set in accordance with the isopach maps, which has comprised all of the effective shallow marine deposits. The position of the boxes with the HST deposits on the Adriatic shelf is shown in Figure 6-12. The preserved sediments have been extracted from the isopach maps and mass balance was estimated at each box. The difference between the amount of fluvial supply and the preserved deposits was considered as an output flux of the first box; and the fluvial supplies to next box plus output flux of the preceding box have been considered as an input flux to the respective boxes. The calculated average sediment fluxes of the HST with their uncertainties (standard deviation, σ) are summarized in Table 6-1 and Table 6-2. The sediment mass balance of the HST-1 deposits shows a total of 27Mt yr^{-1} of sediments has been transported along the western shelf. Total fluvial amount of 53.77 Mt yr^{-1} (~ 274 Gt) was deployed between 5.5 kyr BP and 0.4 kry BP, from which 46.6 Mt yr^{-1} (~238 Gt) has been preserved. The remaining sediment mass of ~13 % were considered as materials drifted south of box 5.

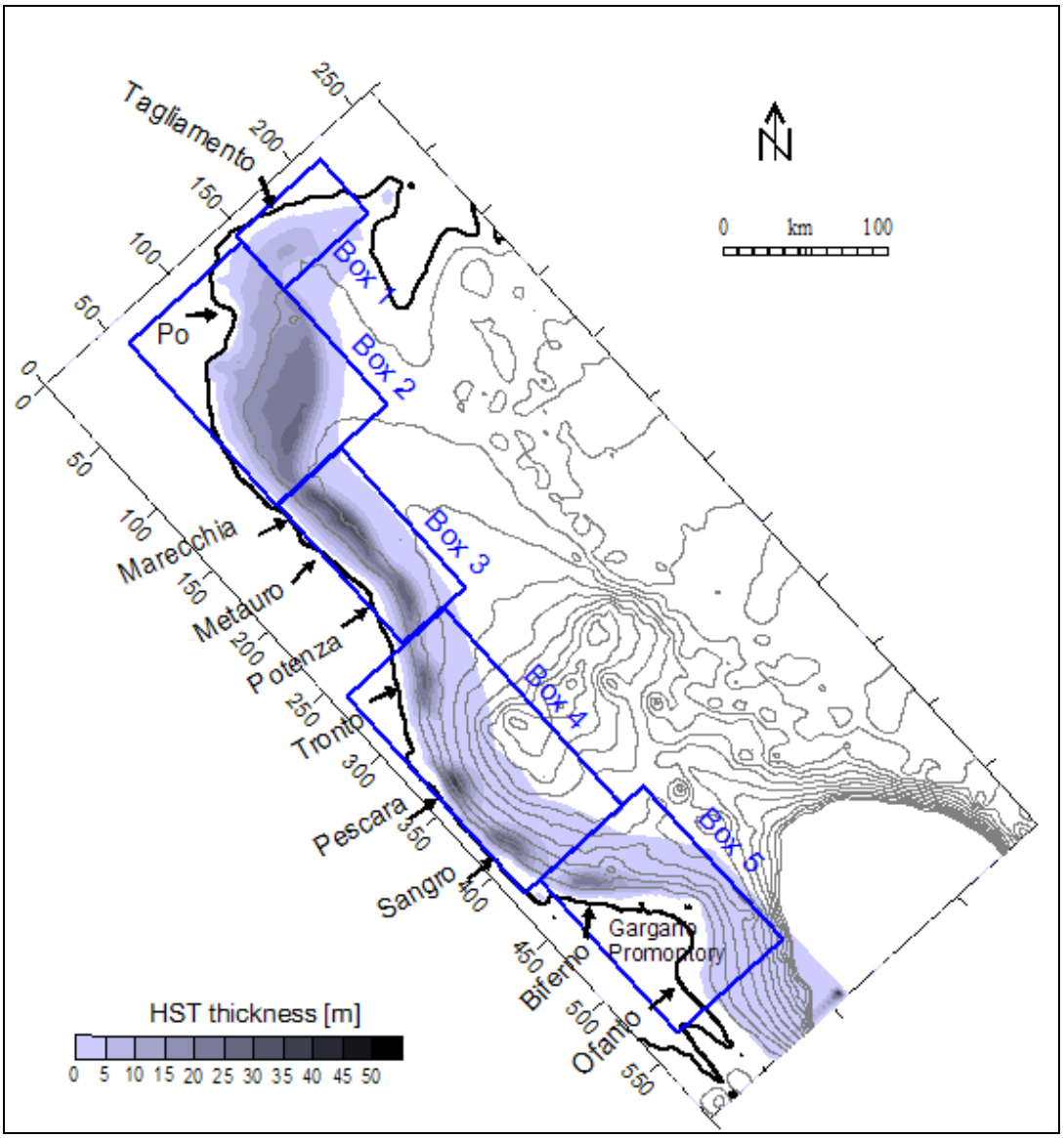

Figure 6-12: Position of boxes on the HST shelf sediments

Table 6-1: HST-1 average sediment mass balance and uncertainties (± σ) along the western shelf

Boxes	Input flux [Mt yr^{-1}]	Mean deposition			Output flux [Mt yr^{-1}]
		[Mt yr^{-1}]	[Mt]	±σ [Mt]	
Box 1	1,7	1,4	6953	0,46	0,4
Box 2	28,1	21,6	110138	2,16	6,5
Box 3	17,8	11,0	56003	1,05	6,8
Box 4	15,9	9,9	50295	0,79	6,1
Box 5	10,0	2,8	14278	2,38	7,2
Total		46,6	237667	6,84	27,0

Table 6-2: HST-2 average sediment mass balance and uncertainties (± σ) along the western shelf

Boxes	Input flux [Mt yr^{-1}]	Mean deposition			Output flux [Mt yr^{-1}]
		[Mt yr^{-1}]	[Mt]	±σ [Mt]	
Box 1	1,7	0,4	192	0,51	1,3
Box 2	18,7	15,5	7741	3,98	3,2
Box 3	13,2	9,0	4524	0,22	4,1
Box 4	13,2	8,9	4445	0,50	4,4
Box 5	8,3	3,0	1484	1,00	5,3
Total		36,8	18385	6,20	18,3

The sediment mass balance of the HST-2 deposits has indicated about 18 Mt yr^{-1} of net sediment has been moved along the shelf. About 42Mt yr^{-1} (~21 Gt) of fluvial sediments were applied and ~37Mt yr^{-1} (~18Gt) has been preserved on the shelf. The remaining 12.6 % of the sediments was considered to move south of box 5. Both systems provided a similar percentage of transported or preserved sediments. The reduction of flux during the HST-2 unit is consistent with the reduction of the fluvial supply.

Depositional rates of the TST deposits were also estimated for the three TST lithosomes and the mean values of the deposits are shown Table 6-3. During the TST-1 system, the total preserved mass, (below the 80m isobath that was the paleo-shore), has exceeded the total fluvial supplied by about 38 Gt. This excess material could have two possible sources. 1) The wave action has a strong effect in digging-out the seafloor sediments of the steep paleo-shorelines of the MAD, and 2) all the rivers north of the MAD could have eroded the formerly exposed part of northern epicontinental shelf. During the latter two systems tracts, the shelf area has preserved more deposits and has reached to 70% at the end of the TST-3 unit. This indicates the development of the Adriatic deposits during the transgression of the sea along the shallower shelf since 14 kyr BP.

The sediment mass of the complete Adriatic system (TST+HST) has also been assessed and is shown in Table 6-4. About 91% of the fluvial supplied material has been deposited within the system, where 59% were preserved on the shelf area of the basin. Sediment masses of the HST and TST units have also been extracted separately, with almost identical results with the values of Table 6-1 and Table 6-3 of their respective systems.

Table 6-3: Total mean sediment mass estimation of the TST units with uncertainties (± σ [Gt])

Lithosome	River supply [Gt]	Total mean deposition		Deposition on the shelf		On shelf %
		[Gt]	±σ [Gt]	[Gt]	±σ [Gt]	
TST-1	143	181	0,02	54	0,02	38
TST-2	140	133	0,09	87	0,03	62
TST-3	220	173	0,07	155	0,06	70
Total	502	487	0,26	295	0,12	59

Table 6-4: Total mean sediment mass estimation of the complete system of TST + HST

Lithosome	River supply [Gt]	Total deposits		On shelf		On shelf %
		[Gt]	±σ [Gt]	[Gt]	±σ [Gt]	
HST+TST	797	727	0,06	472	0,11	59
TST	502	484	0,06	260	0,12	52
HST	295	-	-	243	0,02	82
TST (from table 6.3)	502	487	-	295	-	59
HST (from table 6.1+6.2)	295	254	-	254	-	87

During volume calculations, the boundary of the preserved sediment was chosen so as to enclose all the materials dispersed on the shelf and in the MAD. Different possible boundary lines; that represent the paleo-shorelines have been assessed and have an uncertainty of ±2 Gt form the total Adriatic sediment mass. This shoreline uncertainty and the uncertainties given from Table 6-1 through Table 6-4 are regarded within measurement errors.

Chapter 7: Discussion and Conclusion

The rivers supply rates of Table 5-1 are determined from stratigraphic data and are considered as deterministic values. The sediment amounts were then consistent in all of the simulation scenarios and the calibration focussed on the marine parameters. The liquid discharges were also adjusted so as to carry the sediments to the basin. The leading line of the no-current flowing boundary has been set lower about 60 to 100 km from the coastline of each time step. This has allowed sufficient current flux to pass between the current boundary and the shoreline, which was crucial in sediment transportation. On Figure 5-3, the present day current condition is displayed. Around Gargano promontory an anti-gyres flow field are identified. These current fields could be results of the relative position of the southern rivers that are offset compared to the general current fields and their liquid discharge magnitude may have been exceeded the general flow potential of the basin. Far offshore, the momentum of the sea-current has dominated and these features were diminished. This anticlockwise circulating large-scale oceanic current was simulated and has represented the WACC. The map is comparable with Adriatic surface-water circulation maps of Poulain (2001) and Harris et al. (2008).

Scenario-1 has been chosen as the most realistic scenario for the Adriatic simulation. The isopach maps for the complete TST+HST simulation have revealed two separate types of sedimentation and transportation patterns, Figure 6-5. These were the deposited on the northwest shallow shelf and the sediments on central and western part of the MAD, (central Apennine part of the western shelf). These patterns are formed due to the nature of shelf and the effects of the hydrodynamic conditions. These depositional patterns could be discussed discretely as:

- *Highstand deposits*: The northwest shelf depocenter was characterized by a shore hugging elongated subaqueous stratigraphy. It was formed on the low gradient shelf, shallow water depth and a long basin-ward curved (convex) coastline. These conditions have exposed the clastic sediments to the wave and current actions of the model, and allowed enough time for the routine to re-suspend and disperse the deposits farther till they were removed from suspension and deposited on their final depositional area.

- *Lowstand and Transgressive deposits:* The central Apennine part of the western shelf and the MAD depo-centres were characterized by fan-shaped plum deposits with a minor subaqueous delta features near the Gargano promontory. The shelf has a steep gradient with deep-water and a landward curved shoreline. The high gradient of the shelf has decreased the influence of the hydrodynamic conditions of the model to be less effective to rework and transport the submerged sedimentary bodies (see also Chapter 4:).

Further assessment of the current field, the current potential flow has a constantly decreasing gradient throughout its circulation path in the basin, Figure 7-1. From the figure, it is obvious that there has been a difference of current magnitude between the northern and the central shelf. This difference has also an impact on transport dynamics and could have resulted in the unrealistic stratigraphy and morphology of the central depocenter.

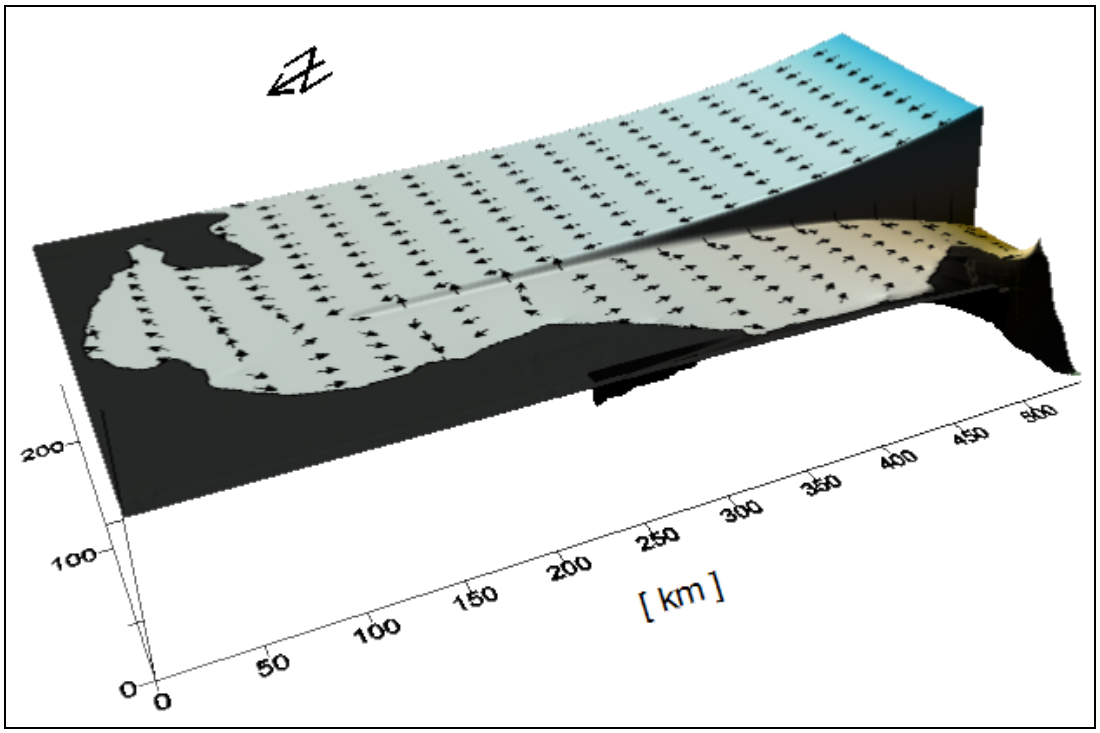

Figure 7-1: Potential flow, decreasing gradient of the current field along the western Adriatic basin.

In the isopach maps of all scenarios there is an erosional zone of about 4 to 6 km offshore of the coasts. This removal or non-deposition of sediments was a typical effect of the wave action. The effects were also evident in the cross-sections where the wave has eroded the coastal zones regardless of the shelf gradient. Far from the shore, thicker deposits have been truncated and flat topsets were created. The fine materials were moved to the foresets and a relatively longshore prograding deposit was formed. A major subaqueous delta was developed about 20 km south of the Po River. This deposit was formed by the Po river supply and represents the subaqueous Po Delta.

The spatial grain-size distribution of the different scenarios shows a large variation compared with the stratigraphic difference among the scenarios. The coarse patches in scenario-2 and scenario-1 correspond to the river positions and were consistent with the isopach maps. The northern shelf deposits, demonstrated a fining trend to both cross-shore and longshore directions. It also proved that the sandy materials are very

close to the coastline and have moved relatively to the south from their respective river positions. This feature could indicate that the shore hugging progradation of the subaqueous delta has segregated grain sizes transportation. The coarse patches on the TST units could indicate positions of paleo-deltas which were retrograding or submerged during the transgression.

The fluvial supply data was preferentially extracted from reports on preserved materials within the Adriatic system rather than present day model estimated supplies. The quantities in Table 5-1 are average values that represent the sediment mass of the Adriatic basin as reported in (Brommer et al. 2009, Syvitski et al. 2007 and Frignani et al. 2005). This technique has reduced the uncertainty in mass estimation and in the simulation of the stratigraphy, since the Adriatic is nearly a closed system. The HST deposits were developed on the well-preserved shallow shelf, which has been subjected to the hydrodynamic conditions of the sea. Thus the sediment flux has been assessed on the result of the HST units. The assessment has estimated about 256 Gt (87% of the supplied fluvial sediments) have been preserved on the western shelf at a rate of ~46 Mt yr^{-1}. It was about 2 to 4 Mt yr^{-1} more than reported in literature (Brommer et al. 2009 and Frignani et al. 2005). The characteristics of the seafloor surface material have a minimal effect on the basin wide sediment masses. The substrate differences have accounted for about ±2 Mt yr^{-1} of sediment flux along the western shelf. The paleo-shorelines delineation has also uncertainty of about ±2 Gt on the net basin wide sediment mass. These uncertainties were within the measurement error and are negligible. The boxes of Figure 6-12 have been made big enough so they contain all the materials delivered from the rivers and were small to exclude deep marine deposits. Uncertainty assessment on their positions and sizes indicated there were very small mass variations that were worthy to disregard. Therefore, the estimated sediment volumes could be considered as acceptable mass results of the model. The unpreserved sediments were considered to move south of box 5. Though some consideration should be accounted for the materials that have been carried offshore of the boxes.

Generally, all the results of the hydrodynamic conditions, sedimentary architecture and grain size distributions presented on the report have basically captured the essence of sediment transport processes and stratigraphic architecture of the Adriatic basin. The results show similar features compared to the isopach maps of Brommer et al. (2009). The results of both models for the complete HST and TST-3 units, which were developed on the north-western shallow shelf, have common stratigraphic features (Figure 6-1 and Figure 2-6). The deposits are characterised by a subaqueous alongshore progradation and has a maximum thickness of about 45 m. The results of both models on the stratigraphic morphology of the central Apennine part of the western shelf are completely different. This shelf area in the maps of Brommer et al. (2009) are characterised by a narrow, continuous and more than 60m thick deposits. While the results of the numerical model illustrated that most of the sediments have preserved on the central part of the MAD and the western shelf has a channel type deposits. The spatial grain-size distribution has also some similarity with the distribution maps of

Brommer (2009), (Figure 6-7 and Figure 2-5). In both models, near the Po delta and close to the northern shoreline, the sediments are coarse; and along the central Apennine coast, the surface sediments demonstrate longshore fining trend. Moreover, south of the Gargano Promontory the sediments appear to be coarser, which reflects a local riverine input.

Finally, from the results and discussions of the study, the following concluding points are summarized:

- The WACC was simulated and was comparable to literature.
- Wave reworking was the most effective hydrodynamic factor of the model and its impact on stratigraphy is highly pronounced.
- Erosional patterns seem to reflect adjustments of the assumed initial seafloor surface sediment to hydrodynamic conditions.
- The stratigraphic units were realistically simulated on a low gradient shelf with a linear shoreline.
- Sediments on a steep sloped marine floor (like the MAD) are less affected by the hydrodynamics, since the sediments were preserved below the wave/current base.
- Materials of the HST system above the wave base bypass the delta front area and moved to the prodelta through the coast hugging currents.
- Spatial grain-size dispersion maps have illustrated cross-shore and longshore fining, which reflects size-selective transport under the dominant hydrodynamic conditions.
- Total sediment mass of about 300 Gt was applied during the HST and about 87% of the sediments were preserved on the shelf.
- The uncertainty in mass balance generated by the seafloor surface materials and delineation of the paleo-shore boundary was minimal compared to the entire basin size (600*264 km) and the total sediment budget (~800 Gt).
- The results of the model have similarity with maps of Brommer et al. (2009) especially on the stratigraphy of the north-western shelf, and the spatial grain size distributions along the western shelf.
- It is not advisable to use a single parameter values for a specific basin; rather combinations of factors (boundary conditions) should be used to mimic the desired morphologic and stratigraphic formations.
- The model is very expensive in terms of the working hours it requires. Hence, well-shaped scenario files with all of the optimal input parameters should be prepared.

The Adriatic basin is a semi closed system that serves as a natural laboratory to calibrate a model. The results of the numerical model on the stratigraphy (especially on the northern shelf); the spatial grain size dispersions and the sediment mass balance on the western shelf are reasonable and suggest that it is possible to simulate the Late Quaternary stratigraphic history and the sediment flux record of the Adriatic basin. The results are also comparable with literature reports as shown in chapter 2.

The model also provides intuitive understanding of stratigraphic and sedimentological processes. Here are some advantages and learning points related to the application of the model:

- It is a flexible method of analyzing a stratigraphy and grain size distribution at various spatial and temporal scales.
- It is possible to evaluate the development of a sedimentary basin by tracing sediment dispersals through the spatial grain size distribution.
- It can be alternatively turned on/off any of the fluvial and/or marine factors to perceive each factor's influence on the stratigraphy of a basin.
- The model can also be used in predicting and monitoring a coastal zone of a sedimentary basin subjected to storm events.

Chapter 8: Recommendation

The results of the different scenarios which are designated to simulate the stratigraphic record of the Adriatic basin have indicated the need for improvement of various components of the model. To precisely reproduce the mud wedge formation on the western Adriatic shelf, some parameters of the model need to be further developed. Hence, it is practical to recommend the following points.

- The shoaling effect of the wave algorithm should be modified for lesser removal of sediments near the coast; and the offshore diffusion needs to be reduced to mimic shore-hugging sedimentation.
- To reproduce a continuous and elongated subaqueous stratigraphy on high gradient shelf, a proper balance between wave reworking and current induced material transportation is required.
- The plume routine might be forcibly diffuse parallel to the shoreline in order to simulate the continuous mud deposits along the central Apennine part of the western shelf.
- For effective longshore sediment transportation, the current routine might also be modified to flow southerly within a defined offshore extent at a constant rate; rather using a circulating and linearly decreasing routine.
- The area just north of the Gargano promontory is characterized by tectonically induced thick deposits. The model should include tectonic/subduction influenced depositional routine in order to simulate such environments.
- It would be helpful to be able to trace the provenance of a riverine material in a basin.
- If possible, the model should simulate multiple grain size classes instead of either coarse or fine ends.
- The Adriatic basin experiences seasonal counter-WACC flux during summer. It would be wonderful if the next version of the model includes such sub-temporal current switcher.

Acknowledgments

Most of all, I am very thankful to the Almighty Lord Christ, who graciously guided me to complete my studies. I am very grateful to Dr. Gert Jan Weltje, with whom the work was carried out with great contribution and supervision. I also extend my gratitude to Rory A.F. Dalman for his close monitoring and crash course on application of the model. Appreciations also to Marit B. Brommer and Joep E.A. Storms who supported me with the model input data. Finally but not least, special thanks to the Delft University of Technology especially the Department of Geotechnology in providing me with all of the research facilities and opportunity to complete my graduate studies.

Reference:

Artegiani, A., Bregant, D., Paschini, E., Pinardi, N., Raicich, F., and Russo, A., (1997). The Adriatic Sea general circulation. Part I: Air–sea interactions and water mass structure. *J. Physical Oceanography, vol. 27, 1492–1514*.

Artegiani, A., Bregant, D., Paschini, E., Pinardi, N., Raicich, F., and Russo, A., (1997). The Adriatic Sea General Circulation. Part II: Baroclinic Circulation Structure. *J. Physical Oceanography, vol. 27, 1515-1532*.

Brommer, M.B., Weltje, G. J., and Trincardi, F., (2009). Reconstruction of sediment supply from mass accumulation rates in the Northern Adriatic Basin (Italy) over the past 19,000 years. *Jo. Geophysical Res., vol.114, 1-15.*

Brommer, M.B., (2009). Mass-balanced stratigraphy. Data-model comparison within a closed sedimentary system (Adriatic Sea, Italy). *PhD thesis*.

Cattaneo, A., Correggiari, A., Langone, L., and Trincardi, F., (2003). The late-Holocene Gargano subaqueous delta, Adriatic shelf: sediment pathways and supply fluctuations. *Marine Geology, vol. 193, 61-91*.

Cattaneo, A., Correggiari, A., Marsset, T., Thomas, Y., Marsset, B., and Trincardi, F., (2004). Seafloor undulation pattern on the Adriatic shelf and comparison to deep-water sediment waves. *Marine Geology, vol. 213, 121-148.*

Cattaneo, A., Trincardi, F., Asioli, A., and Correggiari, A., (2007). The Western Adriatic shelf clinoform: energy-limited bottomset. *Continental Shelf R., vol. 27, 506-525.*

Correggiari, A., Trincardi, F., Langone, L., and Roveri, M., (2001). Styles of failure in Late Holocene Highstand and prodelta wedges on the Adriatic shelf. *Jo. Sedimentary Res., vol. 71, 218-236*

Correggiari, A., Cattaneo, A., and Trincardi, F., (2005). The modern Po Delta system: Lobe switching and asymmetric prodelta growth. *Marine Geology, vol. 222-223, 49-74.*

Dalman, R., and Weltje, G., (2008). Sub-grid parameterisation of fluvio-deltaic processes and architecture in a basin-scale stratigraphic model. *Computers and Geosciences, vol. 34, 1370-1380.*

Dalman, R., (2009). Multi-scale simulation of fluvio-deltaic and shallow marine stratigraphy. *PhD thesis*.

Fain, A., Ogston, A., and Sternberg, R., (2007). Sediment transport event analysis on the western Adriatic continental shelf. *Continental Shelf R., vol. 27, 431-451.*

Farabegoli, E., Onorevoli, G., and Bacchiocchi, C., (2004). Numerical simulation of Holocene depositional wedge in the southern Po Plain-northern Adriatic Sea (Italy). *Quaternary international, vol. 120, 119-132.*

Fleming, K., Johnston, P., Zwartz, D., Yokoyama, Y., Lambeck, K., and Chappell, J., (1998). Refining the eustatic sealevel curve since the Last Glacial Maximum using far- and intermediate-field sites. *Earth and Planetary Science, vol. 163, 327-342.*

Fox, J., Hill, P., Milligan, T., Ogston, A., and Boldrin, A., (2004). Floc fraction in the waters of the Po River prodelta. *Continental Shelf R., vol. 24, 1699-1715.*

Frignani, M., Langone, L., Ravaioli, M., Sorgente, D., Alvisi, F., and Albertazzi, S., (2005). Fine-sediment mass balance in the western Adriatic continental shelf over a century time scale. *Marine Geology, vol. 222-223, 113-133.*

Golden software Inc, (2002). Contouring and 3D Surface Mapping for Scientists and Engineers. *Surfer 8 User's guide, 163-195.*

Harris, C., Sherwood, C., and Signell, R., (2008). Sediment dispersal in the northwestern Adriatic Sea. *Jo. Geophysical Res., Vol. 113.*

Holton, J., (1999). Four geologic settings dominate oil, gas fields of Italy, Sicily. *Oil and Gas- Exploration journal, 81-84.*

Mikkelsen, O., Hill, P., and Milligan, T., (2007). Seasonal and spatial variation of floc size, settling velocity, and density on the inner Adriatic Shelf (Italy). *Continental Shelf Res., vol. 27, 417-430.*

Milligan, T., and Cattaneo, A., (2007). Sediment dynamics in the western Adriatic Sea: From transport to stratigraphy. *Continental Shelf Res., vol. 27, 287-295.*

Milligan, T., Hill, P., and Law, B., (2007). Flocculation and the loss of sediment from the Po River plume. *Continental Shelf Res., vol. 27, 309-321.*

Paschini, E., Artegiani, A., and Pinardi, N., (1993). The mesoscale eddy field of the Middle Adriatic Sea during fall 1988. *Deep Sea Research, vol. 40, 1365-1377.*

Poulain, P.M., (2001). Adriatic Sea surface circulation as derived from drifter data between 1990 and 1999. *Journal of Marine Sciences, vol. 29, 3-32.*

Puig, P., Ogston, A., Guillen, J., Fain, A., and Palanques, A., (2007). Sediment transport processes from the topset to the foreset of a crenulated clinoform (Adriatic Sea). *Continental shelf Res., vol. 27, 452-474.*

Royden, L., Patacca, E., and Scandone, P., (1987). Segmentation and configuration of subducted lithosphere in Italy; an important control on thrust-belt and foredeep-basin evolution. *Jo. Geology 15, 714-717.*

Storms, J., Weltje, G., Terra, G., Cattaneo, A., and Trincardi, F., (2008). Coastal dynamics under conditions of rapid sealevel rise. Late Pleistocene to Early Holocene evolution of barrier– lagoon systems on the northern Adriatic shelf (Italy). *Quaternary Science Reviews, vol. 27, 1107-1123.*

Syvitski, J., Kettner, A., Correggiari, A., and Nelson, B., (2005). Distributary channels and their impact on sediment dispersal. *Marine Geology, vol. 222-223, 75-94.*

Syvitski, J., and Kettner, A., (2007). On the flux of water and sediment into the Northern Adriatic Sea. *Continental Shelf Res., vol. 27, 296-308.*

Trincardi, F., Correggiari, A., and Roveri, M., (1994). Late Quaternary transgressive erosion and deposition in a modern epicontinental shelf: the Adriatic Semienclosed Basin. *Geo-Marine Letters 14, 41-51*.

Wang, X., Pinardi, N., and Malacic, V., (2007). Sediment transport and resuspension due to combined motion of wave and current in the northern Adriatic Sea during a Bora event in January 2001: A numerical modelling study. *Continental Shelf Res., vol. 27, 613-633*.